Journal of Theoretical Biology 439 (2018) 86–99

Contents lists available at ScienceDirect

Journal of Theoretical Biology

journal homepage: www.elsevier.com/locate/jtbi

Activation of the HGF/c-Met axis in the tumor microenvironment: A multispecies model

Anna Konstorum[a,*], John S. Lowengrub[b,c,d,e]

[a] Center for Quantitative Medicine, UConn Health, Farmington, CT, USA
[b] Department of Mathematics, University of California, Irvine, CA, USA
[c] Center for Complex Biological Systems, University of California, Irvine, CA, USA
[d] Department of Biomedical Engineering, University of California, Irvine, CA, USA
[e] Chao Family Comprehensive Cancer Center, University of California, Irvine, USA

ARTICLE INFO

Article history:
Received 30 June 2017
Revised 24 October 2017
Accepted 30 November 2017
Available online 5 December 2017

Keywords:
Cancer
Stem cell
Microenvironment
Multiscale
Computational model
Feedback regulation
Cancer therapy

ABSTRACT

The tumor microenvironment is an integral component in promoting tumor development. Cancer-associated fibroblasts (CAFs), which reside in the tumor stroma, produce Hepatocyte Growth Factor (HGF), an important trigger for invasive and metastatic tumor behavior. HGF contributes to a pro-tumorigenic environment by activating its cognate receptor, c-Met, on tumor cells. Tumor cells, in turn, secrete growth factors that upregulate HGF production in CAFs, thereby establishing a dynamic tumor-host signaling program. Using a spatiotemporal multispecies model of tumor growth, we investigate how the development and spread of a tumor is impacted by the initiation of a dynamic interaction between tumor-derived growth factors and CAF-derived HGF. We show that establishment of such an interaction results in increased tumor growth and morphological instability, the latter due in part to increased cell species heterogeneity at the tumor-host boundary. Invasive behavior is further increased if the tumor lowers responsiveness to paracrine pro-differentiation signals, which is a hallmark of neoplastic development. By modeling anti-HGF and anti-c-Met therapy, we show how disruption of the HGF/c-Met axis can reduce tumor invasiveness and growth, thereby providing theoretical evidence that targeting tumor-microenvironment interactions is a promising avenue for therapeutic development.

1. Introduction

The tumor microenvironment consists of vascular endothelial cells, pericytes, immune inflammatory cells, and cancer associated fibroblasts (CAFs), all which contribute to the hallmarks of cancer (Hanahan and Coussens, 2012; Hanahan and Weinberg, 2011). CAFs include both tissue-derived fibroblasts and recruited myofibroblasts, and promote tumor invasion and metastasis via secretion of growth factors and extracellular matrix (ECM) components (Bhowmick et al., 2004; Kalluri and Zeisberg, 2006). CAF-derived Hepatocyte Growth Factor, HGF, contributes to a pro-tumorigenic environment by activating its cognate receptor, c-Met. High HGF/c-Met activity has been identified in a large number of cancers and is correlated with more severe tumor grade and poor patient survival (Christensen et al., 2005; Matsumoto and Nakamura, 2006; Organ and Tsao, 2011). The signaling cascades triggered by c-Met include the PI3K/AKT, ERK/MAPK, NF-κB, Wnt/β-catenin, and STAT/JNK pathways, among others. These and other cascades contribute to a complex phenotypic response to HGF, which also depends on the cell type and culture conditions. Nevertheless, common responses of tumor cells include increased anchorage-independent growth, motility, and proliferation. Indeed, HGF was first termed Scatter Factor for its scattering effect on epithelial cells (Stoker and Perryman, 1985). Moreover, epithelial tubulogenesis is also observed in some cell types (Birchmeier et al., 2003; Organ and Tsao, 2011; Trusolino et al., 2010). Tumor cells secrete growth factors, including PDGF, TNFα, bFGF, and others (depending on tumor-type) that upregulate HGF production in CAFs (De Luca et al., 2010; Matsumoto and Nakamura, 2006), thereby establishing a dynamic tumor-host signaling program.

An additional heterogeneity in tumors results from intratumoral cell hierarchies, which are generally less robustly controlled and more heterogeneous than in normal tissues (Medema, 2013; Schatton et al., 2009). *In vitro* research on both primary tumor cells and established cancer cell lines has resulted in emergence of cancer stem cells (CSCs) as potential targets of new cancer therapeutics

* Corresponding author.
E-mail addresses: konstorum@uchc.edu (A. Konstorum), lowengrb@math.uci.edu (J.S. Lowengrub).

https://doi.org/10.1016/j.jtbi.2017.11.025
0022-5193/

(Jordan et al., 2006). CSCs are currently regarded as a highly dynamic population, whose behavior is determined by both genetic and environmental factors, and may be, instead of a specific cell type amenable to therapeutic targeting, a phenotype that a large population of cancer cells can achieve in the appropriate environmental conditions (Kreso and Dick, 2014; Zeuner et al., 2014).

Mathematical models of tumor growth now compose several classes, including continuous, discrete, and hybrid; single compartment and multi-compartment (see Byrne, 2010; Deisboeck et al., 2011; Lowengrub et al., 2010; Wang et al., 2015, for comprehensive reviews of the aforementioned model types). Incorporation of the microenvironment into these models involves adding an extra layer of complexity to an underlying model structure. Angiogenesis, macrophage infiltration, and stromal-mechanical perturbations have all been modeled by one or more of the previous model classes (Anderson et al., 2006; Eftimie et al., 2011; Eikenberry et al., 2009; Frieboes et al., 2013; Katira et al., 2013; Rejniak and McCawley, 2010; Welter and Rieger, 2013; Yan et al., 2017; 2016). Many of these modeling studies also include simulation of drug action in the complex milieu of the microenvironment. For example, Eikenberry et al. (2009) developed a partial differential equation model to investigate how surgical resection of a primary melanoma, along with its associated immune cells, would impact the stability of local metastases by disrupting the immune suppression induced by the primary tumor-resident immune cells. The model incorporated tumor-immune interactions into a spatially explicit system that could elucidate how therapy would impact the complex interplay of primary and satellite tumor cells with the immune response.

Despite the prevalence of tumor and tumor-microenvironment models, based on our current knowledge, no tissue-level models of CAF-tumor interactions have been developed that specifically addresses the HGF/c-Met and tumor-derived growth-factor signaling pathway dynamics. Using, as a starting point, a spatiotemporal, multispecies model of tumor growth that accounts for feedback signaling between CSCs and non-CSCs (Yan et al., 2017; 2016; Youssefpour et al., 2012), we investigate how the development and spread of a tumor is impacted by a dynamic interaction between tumor-derived growth factors and CAF-derived HGF, and the physiological effect of therapies directed at reducing the strength of this feedback mechanism.

2. The mathematical model

2.1. Overview

A multispecies continuum model of tumor growth with lineage dynamics and feedback regulation was developed by Youssefpour et al. (2012), who investigated two-stage lineages primarily in two dimensions and Yan et al. (2016), who investigated three-stage lineages in three dimensions. One-way coupling of HGF to tumor dynamics was investigated by Yan et al. (2017), where a non-monotonic effect of external HGF treatment on tumor shape was shown: a low dose increased morphological asymmetry, whereas a higher dose resulted in a larger, but more morphologically stable tumor. In this work, we extend the investigation of HGF-mediated tumor growth by developing a model that incorporates a dynamic, two-way coupling between the tumor and HGF-producing CAFs (Fig. 1). The tumor tissue is modeled to be composed of three cell types: stem, terminal, and dead. While many cell lineage models also include committed progenitor cells as an intermediate phenotype between stem and terminal cells, our model classifies both committed progenitor and cancer stem cells in the stem cell category. We do this in order to lower the parameter burden and to simplify the model. In future work, we will consider these two compartments separately.

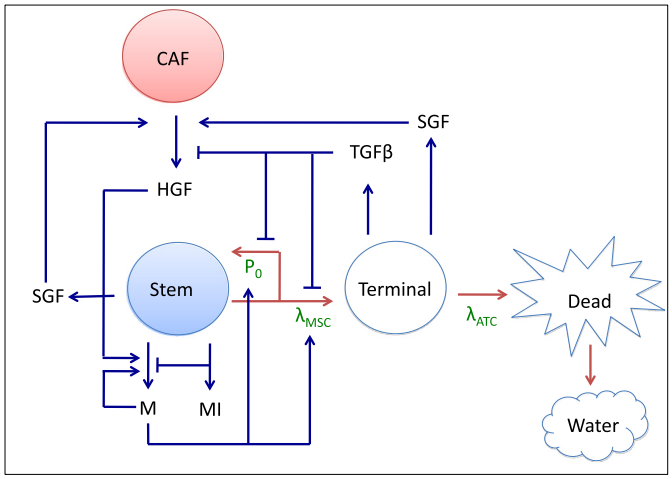

Fig. 1. Tumor-CAF interaction model. Tumor components (water and stem, terminal, and dead cells) are in blue, the host component (CAF) is in red, and associated growth factors and proteins (c-Met (M), c-Met inhibitors (MI), HGF, SGF, TGFβ, and SGF) are in black. Critical parameters are in green, red arrows represent tumor species interconversion, and blue arrows represent chemical production and action. Stem cells renew with probability P_0 and divide with rate λ_{MSC}. Terminal cells die at a rate λ_{ATC} and dead cells are converted to water. P_0 is promoted by products of the c-Met signaling cascade (M) and HGF, and lowered by TGFβ, which is produced by the terminal cells. c-Met production, in turn, is promoted by itself and HGF, and lowered by c-Met inhibitors (MI). HGF production by CAFs is promoted by SGF, which are produced by stem and terminal cells. (For interpretation of the references to color in this figure legend, the reader is referred to the web version of this article.)

Stem cells have a probability of self-renewal, P_0, and a division rate, λ_{MSC}, that are dependent upon negative feedback from TGFβ family members produced by terminal cells and positive feedback from products of the c-Met signaling cascade. Stem cell scatter and motility are also increased by c-Met (not shown in Fig. 1). Additionally, c-Met is inhibited by stem-cell produced c-Met inhibitors. Cancer-associated fibroblasts, CAFs, reside in the host tissue, and interact with the tumor by secreting HGF, which is stimulated by release of stroma-acting growth factors (SGF) by the stem and terminal cells. HGF, in turn, promotes production of c-Met products. Terminal cells die at a rate λ_{ATC}, and dead cells are eventually converted to water (Fig. 1).

2.2. Cell species conservation, HGF-induced cell spread, and cell velocity

Local area fractions of the cell species ($\phi_{CSC,\,TC,\,DC}$), host (ϕ_H), and water (ϕ_W) make up the dependent variables, which sum to 1. Assuming that that the total solid and water fractions are constant allows us to determine the water component via solid component dynamics. A conservation equation of the form

$$\frac{\delta \phi_*}{\delta t} = \overbrace{-\nabla \cdot \mathbf{J}_*}^{\text{Generalized Diffusion}} + \overbrace{Src_*}^{\text{Mass-exchange}} + \overbrace{-\nabla \cdot (\mathbf{u}_s \phi_*)}^{\text{Advection}} \tag{1}$$

is assumed for each cell type, where * denotes tumor cell species. A Helmholtz free energy of global adhesion is given by Wise et al. (2008) and Youssefpour et al. (2012)

$$E = \frac{\gamma}{\varepsilon} \int_\Omega F(\phi_T) + \varepsilon^2 |\nabla \phi_T|^2 dx, \tag{2}$$

where Ω is the domain occupied by the tumor and host, $\phi_T = \phi_{CSC} + \phi_{TC} + \phi_{DC}$ is the total solid tumor area fraction, $F(\phi_T)$ models energy from local adhesion, ε models longer range component interactions, and γ is a global measure of cell-cell adhesion (incorporating both local and longer-range contributions to

adhesion). Generalized diffusion for tumor components is represented by $-\nabla\cdot\mathbf{J}_*$, where $\mathbf{J}_* = -M_b\phi_*\nabla\mu$. For the host, we have $\mathbf{J}_H = M_b\phi_T\nabla\mu$. Here, M_b is mobility and μ is the chemical potential,

$$\mu = \frac{\delta E}{\delta\phi_T} = \frac{\gamma}{\varepsilon}\left(\frac{dF}{d\phi_T}(\phi_T) - \varepsilon^2\nabla^2\phi_T\right). \tag{3}$$

Since the first discovery of HGF as a scatter factor for epithelial cells, HGF has been shown to have a pro-migratory effect on cells in the contexts of development, wound healing, and cancer (Birchmeier et al., 2003). The pro-migratory effect is mediated by several pleiotropic effects of activated c-Met on cell physiology. The c-Met-activated Ras cascade has been shown to be critical for disassembly of adherens junctions between tumor cells (Potempa and Ridley, 1998; Ueoka et al., 2000). Additionally, activated c-Met results in increased production of the proteolytic enzyme urokinase-type plasminogen activator (uPA) and its receptor (uPAR) (Jeffers et al., 1996; Nishimura et al., 2003). uPA catalyzes ECM degradation and remodeling, and is correlated with increased malignancy in several cancers (Duffy, 2004; Sidenius and Blasi, 2003; Ulisse et al., 2009). In MDCK cells, HGF-activated c-Met was found to further promote cell dispersal by enhancing cell-ECM interactions via modification of cellular transmembrane integrin protein activity (Trusolino et al., 2000).

We model the effect of c-Met on cell spread by having it act on the local interaction energy, $F(\phi_T)$, as follows. First, we model F as a double-well potential and represent it as a sum of its convex and concave parts, which model cell-cell repulsion (and attraction to ECM), and cell-cell attraction, respectively, with cell-cell adhesion arising from a balance between the two (Wise et al., 2008). We can model the effect of HGF as shifting this balance via its effect on c-Met. Accordingly, we introduce a weighting function $g(C_M)$ and modify F as follows,

$$F(\phi_T) = \frac{\tilde{E}(C_M)}{4}\left(\left(\left(\phi_T - \frac{1}{2}\right)^4 + \frac{1}{16}\right) - \frac{1}{2}\left(\phi_T - \frac{1}{2}\right)^2 g(C_M)\right), \tag{4}$$

$$\tilde{E}(C_M) = 1 + \frac{\delta_2 C_M}{1+\delta_2 C_M}, \tag{5}$$

$$g(C_M) = \frac{1}{1+\delta_1 C_M}, \tag{6}$$

where $\tilde{E} > 0$ is an energy scale and C_M is the concentration of c-Met. When $\tilde{E}(C_M) = g(C_M) = 1$, the original F is recovered. As $g(C_M)$ decreases, F tends towards a single-well potential at $\phi_T = 1/2$. By taking $g(C_M)$ as in (6), where δ_1 is the strength of c-Met effect on g, we can obtain a shift towards the single-well potential with increasing c-Met. This allows us to model the breakdown of cell-cell adhesion and increase in cell-matrix adhesion promoted by c-Met. Additionally, by taking $\tilde{E}$ as in (5), where δ_2 indicates strength of c-Met action on $\tilde{E}$, we can model the local effect of c-Met on ECM remodeling, since an increased $\tilde{E}$ increases the driving force of the components independently of whether F is a single- or double-well potential.

The cell velocity, $\mathbf{u}_s$, is assumed to satisfy the generalized Darcy's law, which is a constitutive equation that models fluid flow through a porous media (Lowengrub et al., 2010; Wise et al., 2008),

$$\mathbf{u}_s = -\kappa\left(\nabla p - \frac{\gamma}{\varepsilon}\mu\nabla\phi_T\right), \tag{7}$$

where κ reflects combined effects of cell-cell and cell-matrix adhesion, p is the solid pressure generated by cell proliferation, and μ is the chemical potential (3). We can sum the conservation equations to obtain an equation for velocity

$$\nabla\cdot\mathbf{u}_S = Src_{CSC} + Src_{TC} + Src_{DC}, \tag{8}$$

with the assumption that the host is under homeostatic conditions ($Src_H = 0$). The pressure p can be obtained by solving Eqs. (7) and (8).

At the far-field boundary, Σ_∞, of the domain, Ω, we impose no-flux, homogeneous Neumann boundary conditions: $\nabla\phi_{T,CSC,TC} = \omega_\infty = 0$, where ω_∞ is the outwards-pointing normal vector on Σ_∞. Chemical potential, μ, and pressure, p, have homogeneous Dirichlet conditions $\mu = p = 0$ on Σ_∞, allowing the tumor to move across the outer boundary (Wise et al., 2008).

2.3. The mass-exchange equations

Src_* represents the mass-exchange terms, which incorporate mitosis, differentiation, death, and species conversion. The self-renewal rate of the CSCs is P_0, and both the self-renewal and mitosis rates are proportional to the concentration of oxygen and nutrients, represented by a single variable C_O. The source terms are as follows:

$$Src_{CSC} = \overbrace{\lambda_{MSC}(2P_0 - 1)\phi_{CSC}C_O G(\phi_{CSC})}^{\text{Cancer stem cell (CSC) self-renewal}}, \tag{9}$$

$$Src_{TC} = \overbrace{2\lambda_{MSC}(1-P_0)\phi_{CSC}C_O G(\phi_{CSC})}^{\text{Differentiation of CSCs}} + \overbrace{\lambda_{MTC}\phi_{TC}C_O G(\phi_{TC})}^{\text{Mitosis}} - \overbrace{\lambda_{ATC}\phi_{TC}}^{\text{Death}}, \tag{10}$$

$$Src_{DC} = \overbrace{\lambda_{ATC}\phi_{TC}}^{\text{Death}} - \overbrace{\lambda_L\phi_{DC}}^{\text{Lysis}}, \tag{11}$$

where mitosis, cell death, and lysis rates are denoted by λ_{M^*}, λ_{A^*}, and λ_{L^*}, respectively, where * indicates cell type. Proliferation is cut off at sufficiently low concentration by $G(\phi_*)$, specifically, we take (Wise et al., 2008; Youssefpour et al., 2012)

$$G(\phi_*) = \begin{cases} 1 & \text{if } \phi_* > \frac{3}{2}\varepsilon, \\ \phi_* - \frac{1}{2}\varepsilon & \text{if } \frac{1}{2}\varepsilon < \phi_* < \frac{3}{2}\varepsilon, \\ 0 & \text{if } \phi_* < \frac{1}{2}\varepsilon. \end{cases} \tag{12}$$

2.4. Stem cell self-renewal and division

HGF/c-Met induces cellular proliferation via multiple signaling cascades, including Ras/Raf, PI3K/Akt, NF-κB, and Wnt/β-catenin (Birchmeier et al., 2003; Li et al., 2015; Muller et al., 2002; Organ and Tsao, 2011; Trusolino et al., 2010). Moreover, HGF/c-Met has been implicated in CSC development and maintenance in colon cancer (Vermeulen et al., 2010), glioblastoma (Joo et al., 2012; Li et al., 2011) and head and neck squamous cell carcinoma (HNSCC) (Lim et al., 2014). For example, Vermeulen et al. (2010) showed that HGF-induced β-catenin nuclear localization and activation of canonical Wnt signal was associated with increased cellular clonogenicity in primary colon cancer spheroid cultures, implicating the cascade in promoting the CSC phenotype. Similarly, Lim et al. (2014) have shown that in HNSCC HGF/c-Met promoted HNCSCC CSC marker expression and cell sphere-forming capacity. When c-Met was knocked down, the cells showed increased radiosensitivity and decreased ability to form tumors in a mouse xenograft model. HGF has also been shown to have an effect on reducing cell death rates (Xiao et al., 2001).

TGFβ is a potent growth inhibitor (Huang and Huang, 2005) and differentiation promoter (Watabe and Miyazono, 2009) for many cell types and early-stage tumors. We model the effect of c-Met and TGFβ on stem cell self-renewal and proliferation below. To lower the parameter burden, we maintain a low, and constant,

apoptotic rate in the Src_* equations that is not dependent on the growth factors. We take

$$P_0 = P_{\min} + (P_{\max} - P_{\min})\left(\frac{\xi_0 C_M}{1+\xi_0 C_M}\right)\left(\frac{1}{1+\psi_0 C_{TGF\beta}}\right), \tag{13}$$

$$\lambda_{MSC} = \lambda_{MSC_{min}} + (\lambda_{MSC_{max}} - \lambda_{MSC_{min}})\left(\frac{\xi_1 C_M}{1+\xi_1 C_M}\right)\left(\frac{1}{1+\psi_1 C_{TGF\beta}}\right), \tag{14}$$

where $C_{TGF\beta}$ is the concentration of TGFβ, and $P_{min,\,max}$ and $\lambda_{MSC_{min,max}}$ are the minimum and maximum rates of self-renewal and CSC division rates, respectively. The strength of the c-Met effect on P_0 and λ_{MSC} is represented by ξ_0 and ξ_1, respectively, while the strength of the inhibitory TGFβ action on P_0 and λ_{MSC} is represented by ψ_0 and ψ_1, respectively.

2.5. Chemical species

2.5.1. Oxygen / nutrients

The combined effect of oxygen and nutrients is denoted as O. Uptake is assumed to be negligible in the host in comparison to the tumor species, and diffusion rapid in comparison to the rate of cell proliferation (Wise et al., 2008; Youssefpour et al., 2012). Hence, the corresponding concentration C_O can be modeled using a quasi-steady state equation,

$$0 = \nabla\cdot(D_O\nabla C_O) - (\nu_{UOCSC}\phi_{CSC} + \nu_{TC}\phi_{TC})C_O + \nu_{PO}(\bar{C}_{AO} - C_O)Q(\phi_T), \tag{15}$$

where ν_{UOCSC}, ν_{UOTC} are the uptake rates by the CSCs and TCs, respectively, and D_O is the diffusion coefficient. The rate of O entering the microenvironment is modeled by ν_{PO}, and the concentration of O in the medium sufficiently far from the tumor is given by $\bar{C}_{AO}$, which is also taken to be the boundary condition on Σ_∞, $C_O = \bar{C}_{AO}$. The host domain is approximated by $Q(c)$, an interpolating function from the tumor ($Q = 0$) to the host ($Q = 1$), and is taken to be (Wise et al., 2008)

$$Q(c) = 3c^2 - 2c^3, \tag{16}$$

where $c = 1 - \phi_T$.

2.5.2. TGFβ

A diffusible differentiation promoter, produced by the terminal cells, is modeled by the variable TGFβ, which represents the TGFβ superfamily (Lombardo et al., 2011; Moses and Serra, 1996). Although in later stages of cancer TGFβ may be produced by other cells (namely stroma and immune), we do not model that here since this progression coincides with inactivation of certain TGFβ downstream signaling components and results in a phenotypically distinct role of TGFβ from its tumor-suppressing effects (Massagué, 2008). We model the loss of responsiveness to TGFβ in Section 3.3 and discuss approaches to modeling the 'TGFβ paradox' (i.e. its tumor-promoting actions) in Section 4.

Rapid diffusion is assumed for TGFβ due to the long-range action of some of its family members, such as Activin (Jones et al., 1996), which is directly involved in regulating epithelial tumorigenesis (Le Bras et al., 2014), or BMP4, which can have an effective long-range gradient due to long-range diffusion of its inhibitors (Dale and Wardle, 1999; Jones and Smith, 1998). Hence, we use a quasi-steady reaction-diffusion equation for $C_{TGF\beta}$,

$$0 = \nabla\cdot(D_{TGF\beta}\nabla C_{TGF\beta}) - (\nu_{UTGF\beta}\phi_{CSC} + \nu_{DTGF\beta})C_{TGF\beta} + \nu_{PTGF\beta}\phi_{TC}, \tag{17}$$

where $\nu_{UTGF\beta}$ is the uptake rate by CSCs, $\nu_{DTGF\beta}$ is the decay rate, $\nu_{PTGF\beta}$ is the production rate by TCs, and $D_{TGF\beta}$ is the TGFβ diffusion coefficient. The boundary condition for $C_{TGF\beta}$ is taken to be Dirichlet ($C_{TGF\beta} = 0$) on Σ_∞.

2.5.3. c-Met and c-Met inhibitors

A generalized Geirer-Meinhardt-Turing system is used to model the interaction of the activator c-Met and its downstream products with their inhibitors (Gierer and Meinhardt, 1972; Turing, 1952). Such a system, with Wnt/Dkk as the activator/inhibitor pair has been suggested in hair follicle development (Sick et al., 2006), crypt generation (Zhang et al., 2012), and tumor development (Youssefpour et al., 2012). The large number of cross-activating downstream signaling components of c-Met, some of which include positive feedback loops amongst themselves (Syed et al., 2011; Verma et al., 2015), motivate a nonlinear c-Met activation term. Inhibitors of c-Met and the downstream effectors activated by induced c-Met include the autocrine-acting c-CBL (Petrelli et al., 2002), paracrine-acting Delta (Stella et al., 2005), and the secreted factor Dkk. Since c-Met products are autocrine or paracrine effectors, we take c-Met products to have a short-range, and c-Met inhibitors a long-range, diffusion coefficient. The functional correlation between cancer stem cells and enhanced c-Met activity has been discussed in Section 2.4, hence we model c-Met and c-Met inhibitor production to be limited primarily to CSCs. We also include low-level background production of c-Met by all viable tumor cell types. Since HGF activates c-Met products and induces c-Met production, we model the effect of HGF on c-Met by its positive effect on the production rate of c-Met. Finally, production is made dependent on nutrient (O) levels (in this model, we do not consider hypoxia-dependent c-Met upregulation (Trusolino et al., 2010)). We take

$$\frac{\partial C_M}{\partial t} = \nabla\cdot(D_M\nabla C_M) + f(C_M, C_{MI}), \tag{18}$$

$$\frac{\partial C_{MI}}{\partial t} = \nabla\cdot(D_{MI}\nabla C_{MI}) + g(C_M, C_{MI}), \tag{19}$$

$$f(C_M, C_{MI}) = \nu_{PM}\frac{\lambda_{2_{HGF}}C_{HGF} + C_M^2}{C_{MI}}C_O\phi_{CSC} - \nu_{DM}C_M + \eta_M C_O(\phi_{CSC} + \phi_{TC}), \tag{20}$$

$$\nu_{PM} = \nu_0 + \lambda_{1_{HGF}}C_{HGF}, \tag{21}$$

$$g(C_M, C_{MI}) = \nu_{PMI}C_M^2 C_O\phi_{CSC} - \nu_{DMI}C_{MI}, \tag{22}$$

where C_M and C_{MI} are the concentrations of c-Met products and c-Met inhibitors, respectively, D_M is the diffusion coefficient for downstream c-Met effectors, which is assumed to be small relative to the diffusion coefficient for c-Met inhibitors, D_{MI}. The strength of positive feedback of HGF on c-Met is represented by $\lambda_{1,2_{HGF}}$, η_M represents background production of c-Met products, ν_{PM}, ν_{DM} are the respective production and decay rates of c-Met-activated proteins and ν_{PMI}, ν_{DMI} are the respective production and decay rates of c-Met inhibitor proteins. The production rate of c-Met-activated proteins, ν_{PM}, is taken to be the sum of ν_0, the auto-activation rate of M, and $\lambda_{1_{HGF}}C_{HGF}$.

We note that we have two HGF-dependent actions on c-Met production, with respective strengths $\lambda_{1_{HGF}}$ and $\lambda_{2_{HGF}}$, due to the multi-modality of HGF action on c-Met and its downstream effectors. In order to better understand how each HGF-dependent action on c-Met affects c-Met product levels and tumor phenotype, we developed a reduced, homogenous model of the system and performed a Turing analysis on it in Appendix A.

We assume no flux, homogeneous Neumann, boundary conditions for c-Met and c-Met inhibitor chemical fields, hence we take $\omega_\infty\cdot\nabla C_M = \omega_\infty\cdot\nabla C_{MI} = 0$ on Σ_∞.

2.5.4. HGF and stroma-acting growth factors (SGF)

Cancer cells secrete growth factors and cytokines such as TNFα, bFGF, and PDGF, which induce upregulation of HGF production in stroma-resident fibroblast cells (De Luca et al., 2010; Gohda et al., 1994; Matsumoto and Nakamura, 2006; Roletto et al., 1996). Because of the lack of definitive data, we cannot currently specify whether the CSCs preferentially release these growth factors, and if increased c-Met signal results in an increased release of these factors, thus we model a positive effect of the growth factors from all viable tumor tissue on HGF production by fibroblasts in the stroma. The fibroblasts are considered to be homogeneously, and densely, distributed within the stroma (Karagiannis et al., 2012), although there is evidence that ECM remodeling occurs at the tumor-host boundary to allow for tumor spread (Friedl and Wolf, 2008), we account for this phenomenon not via changing the host phenotype but by making tumor cells more motile (see Section 2.2).

Additionally, there is substantial evidence that TGFβ is a negative regulator of HGF production in stroma-resident fibroblasts, and thus we include its inhibitory effect in the model (Gohda et al., 1992; Harrison et al., 2000; Matsumoto and Nakamura, 2006):

$$\frac{\partial C_{HGF}}{\partial t} = \nu_{PHGF}\frac{C_{SGF}}{\zeta + C_{TGF\beta}}C_O Q(\phi_T) - \nu_{DHGF}C_{HGF} + \nabla\cdot(D_{HGF}\nabla C_{HGF}), \tag{23}$$

$$\frac{\partial C_{SGF}}{\partial t} = C_O(\nu_{SGFS}\phi_{CSC} + \nu_{SGFT}\phi_{TC}) - \nu_{DSGF}C_{GF} + \nabla\cdot(D_{SGF}\nabla C_{SGF}), \tag{24}$$

where C_{HGF} is the concentration of HGF, ν_{PHGF} and ν_{DHGF} are the respective production and decay rates of HGF, and ζ is a value close to zero added to regularize the equation. The interpolation function $Q(\phi_T) \approx 1 - \phi_T$ is given by Eq. (16), and D_{HGF} is the diffusion coefficient for HGF. D_{HGF} is taken to be smaller than the diffusion coefficients for the other growth factors due to its high molecular weight (Nakamura et al., 1989). The production rates of SGF by the stem and terminal cell fractions are ν_{SGFS} and ν_{SGFT}, respectively. The decay rate is ν_{DSGF} and D_{SGF} is the diffusion rate of the growth factors. In the main text, we let $\nu_{SGFS} = \nu_{SGFT}$, and test the cases where SGF production is significantly higher for the CSC or terminal cell compartment in the Supplementary Material, Section S3.

2.6. Nondimensionalized equations

The equations are nondimensionalized following (Wise et al., 2008; Youssefpour et al., 2012): we take the O diffusion scale, $l = \sqrt{D_O/\nu_{UOSC}}$, and the mitosis time scale $\tau = (\lambda_{MSC_M}\bar{C}_{AO})^{-1}$, where λ_{MSC_M} represents the mean of $\lambda_{MSC_{min}}$ and $\lambda_{MSC_{max}}$. The diffusion length scale, l, is estimated to be $l \approx 150\mu m$ and the mitosis time scale to be $\tau \approx 1$ day following (Frieboes et al., 2006). The nondimensionalization procedure and parameters are described in Supplementary Material, Section S1 and Section 2.7, respectively. Below we show the equations that change after nondimensionalization, where the others are identical with the dimensional forms, except that variables and parameters are redefined, as explained in the Supplementary Material Section S1 and Section 2.7.

The nondimensionalized equations for O and TGFβ, respectively, are

$$0 = \nabla^2 C_O - C_O(\phi_{CSC} + \nu_{UOTC}\phi_{TC}) + \nu_{PO}(1 - C_O)Q(\phi_T), \tag{25}$$

$$0 = \nabla^2 C_{\mathrm{TGF}\beta} - (\nu_{UT}\phi_{CSC} + \nu_{DT})C_{\mathrm{TGF}\beta} + \nu_{\mathrm{PTGF}\beta}\phi_{TC}. \tag{26}$$

The nondimensionalized equations for c-Met and c-Met inhibitors are

$$\frac{\partial C_M}{\partial t} = \nabla\cdot(D_M\nabla C_M) + Rf(C_M, C_{MI}), \tag{27}$$

$$\frac{\partial C_{MI}}{\partial t} = \nabla\cdot(D_{MI}\nabla C_{MI}) + Rg(C_M, C_{MI}), \tag{28}$$

$$f(C_M, C_{MI}) = \nu_{PM}\frac{\lambda_{2_{HGF}}C_{HGF} + C_M^2}{C_{MI}}C_O\phi_{CSC} - C_M + \eta_M C_O(\phi_{CSC} + \phi_{CP} + \phi_{TC}), \tag{29}$$

$$\nu_{PM} = \nu_0 + \lambda_{1_{HGF}}C_{HGF}, \tag{30}$$

$$g(C_M, C_{MI}) = C_M^2 C_O\phi_{CSC} - \nu_{DMI}C_{MI}. \tag{31}$$

2.7. Nondimensionalized model parameters

The nondimensional parameter values used in the model are presented in Tables 1 and 2, for brevity, c-Met is shortened to M and c-Met inhibitors to MI. Since this model is an extension of the Youssefpour et al. (2012) model, with earlier versions published in Konstorum et al. (2013a); 2013b), a majority are derived from these references, as identified by (*) for Youssefpour et al. (2012) and (**) for Konstorum et al. (2013b), in the References column of Tables 1 and 2. Choices of other parameters are discussed in the main text. The reader is referred to the part of the text that address the specific parameter under the References column of Tables 1 and 2.

3. Results

An adaptive finite difference nonlinear multigrid method (Wise et al., 2011; 2008; Youssefpour et al., 2012) is used to solve the governing equations efficiently on a computational domain of $[-20, 20]^2$. We solve for $\phi_T = \phi_{CSC} + \phi_{TC} + \phi_{DC}$, then we can calculate $\phi_{TC} = \phi_T - (\phi_{CSC} + \phi_{DC})$. To remove the high-order time step constraint incurred by an explicit method, we use an implicit 2nd order accurate time discretization of Crank-Nicholson type, and spatial derivatives are discretized using 2nd order accurate central difference approximations. In regions of large gradients, block structured Cartesian refinement is used to provide enhanced local resolution. For further details, see Wise et al. (2011) or Youssefpour et al. (2012).

We initialize the tumor with an asymmetrical shape and a 45/50/5 homogenous fractional distribution of SCs, TCs, and DCs (respectively). We note that changing the initial fractional distribution of cell compartments does not have a qualitative effect on the simulations. The initialized asymmetrical shape can be visualized in the inset in Fig. 2(a), its mathematical formulation is described in the Supplementary Material, Section S2. This initial condition provides a diffuse interface representation of an asymmetrical tumor centered at the origin with maximum radius of $\sqrt{3}$. Choice of a different asymmetrical initial shape does not influence the results in a qualitative manner.

We take initial conditions for C_M and C_{MI}, the concentrations of c-Met and c-Met inhibitor, as identical to those for C_W and C_{WI}, the concentrations for Wnt and Wnt inhibitors, respectively, in Youssefpour et al. (2012) in order to maintain continuity with the former model in the sense that we want the control condition to be qualitatively similar to the model presented therein. We elaborate on our choice of initial conditions for C_M, C_{MI}, as well as for C_{SGF} and C_{HGF} in the Supplementary Material, Section S2. We note that other initial conditions for c-Met, c-Met inhibitor, HGF, and SGF produce qualitatively similar results. Since C_O and $C_{\mathrm{TGF}\beta}$ satisfy quasi-steady diffusion equations, we need not take initial conditions for these fields.

Table 1
Nondimensionalized cell-level parameters (Sections 2.2–2.4, 2.6).

Parameter	Description	Value	Reference
γ	Global adhesion	−0.1	(*)
ε	Diffuse interface thickness	0.05	(*)
M_b	Mobility	10.0	(*)
δ_1	Strength of M effect on $F(\phi_T)$, measure of cell scatter	0.02	Section 3.2
δ_2	Strength of M effect on $\tilde{E}$, the energy scale	0.02	Section 3.2
κ	Pressure-dependent cell motility	1.0	(*)
λ_{MTC}	TC mitosis rate	0.1	(*)
λ_{ATC}	TC death rate	0.1	(*)
λ_L	DC lysis rate	1.0	(*)
P_{min}	Min. CSC self-renewal rate	0.2	(*)
P_{max}	Max. CSC self-renewal rate	1.0	(*)
ξ_0	Strength of M action on P_0	1.0	(*)
ψ_0	Strength of TGFβ action on P_0	1.0	Section 3.1
$\lambda_{MSC_{min}}$	Min. CSC mitosis rate	0.5	Estimated, (Frank, 2007, Chapter 12)
$\lambda_{MSC_{max}}$	Max. CSC mitosis rate	1.5	Estimated, (Frank, 2007, Chapter 12)
ξ_1	Strength of M action on λ_{MSC}	0.5	Estimated by simulation
ψ_1	Strength of TGFβ action on λ_{MSC}	0.5	(**)

Table 2
Nondimensionalized chemical species parameters (Sections 2.5, 2.6).

Parameter	Description	Value	Reference
ν_{UOTC}	Oxygen uptake rate by TCs	1.0	(*)
ν_{PO}	Oxygen transfer rate	0.5	(*)
$\nu_{\mathrm{UTGF}\beta}$	TGFβ uptake rate by CSCs	0.05	(*)
$\nu_{\mathrm{TGF}\beta}$	TGFβ decay rate	0.0	(*)
$\nu_{\mathrm{PTGF}\beta}$	TGFβ production rate by TCs	0.1	(*)
D_M	Diffusion of M effectors	1.0	(*)
D_{MI}	Diffusion of MI effectors	25.0	(*)
ν_0	Strength of HGF-independent M activation	1.0	(*)
$\lambda_{1,2_{HGF}}$	Strength of HGF-induced M activation	0.5	Section 3.2
ν_{DM}	M decay rate	1.0	(*)
η_M	Background M production rate	0.2	(*)
ν_{DMI}	MI Decay rate	1.0	(*)
R	Reaction rate	50.0	(*)
ν_{PHGF}	Strength of SGF on HGF activation	{5,10,15}	Sections 3.1, S3
ν_{DHGF}	HGF decay rate	1.0	(**)
D_{HGF}	HGF diffusion rate	0.1	(**)
ν_{SGFS}	SGF production rate by CSCs	{5,10,15}	Section 3.1, S3
ν_{SGFT}	SGF production rate by TCs	{5,10,15}	Section 3.1, S3
ν_{DSGF}	SGF decay rate	1.0	(**)
D_{SGF}	SGF diffusion rate	1.0	(**)

3.1. Tumor progression with varying HGF feedback

We begin by simulating HGF dynamics in a tumor in its early stages, when response to inhibitory growth feedback is relatively strong. We do this by setting the TGFβ self-renewal feedback parameter, ψ_0, to $\psi_0 = 1$. In Youssefpour et al. (2012), the authors showed that a growing tumor with no HGF feedback and $\psi_0 = 1$ grows slower and is more stable than a tumor with $\psi_0 = 0.5$. In Section 3.3, we will show how HGF feedback alters tumor behavior with lowered response to TGFβ. We incorporate different strengths of HGF feedback (see below) at time $T = 10$ (recall T is measured in CSC cell cycles) in the simulation. We do this since we expect a delay between tumor initialization and microenvironmental recruitment, although there is evidence that in certain cases, mutations in microenvironmental components may drive tumorigenesis (Trimboli et al., 2009). In our system we consider the tumor as the initiator of the microenvironment-tumor interaction. We note that we do not observe qualitative differences between the choice of early T at which to start the HGF dynamics and the resulting tumor phenotype.[1]

Since the strength of the dynamic relationship between HGF and SGF feedback is unknown, we simulate growth of the tumor in four distinct conditions: none, low, intermediate (int), and high HGF feedback. To change the strength of feedback, we focus on three parameters found in Eqs. (23) and (24), ν_{PHGF}, ν_{SGFS}, and ν_{SGFT}. The strength of SGF action on HGF is represented by ν_{PHGF}, and $\nu_{SGFS,T}$ are the respective production rates of SGF by the stem and terminal tissue fractions. For low (respectively, int, high) HGF, we set $\nu_{PHGF} = \nu_{SGFS} = \nu_{SGFT} = 5$ (respectively 10, 15). With HGF dynamics initiated at $T = 10$, the stem cell fractions from the resulting simulations for $T = 50$, 100, and 150 are shown in Fig. 2(a). The outline of the tumor body is clearly visible in all simulations, and is highlighted in green for the no HGF, $T = 50$ case. We see that as HGF dynamics increase from none to int, the number of stem cell spots increases, and there is a change to a more asymmetrical morphology. As HGF dynamics further increase to the high mode, the number of spots decreases, but the spot size increases, and there is a large change in the morphology with an increase in invasive fingering and tumor fragmentation ($T = 150$).

We observe that the rate of increase of total tumor area is positively correlated with increasing HGF strength (Fig. 2(b)(i)),

[1] An exception to this statement occurs if we include HGF dynamics at $T < 2$. During very early time, initial pattern formation occurs, and we have observed that the resulting phenotype becomes highly sensitive to parameter values and specific time of HGF dynamic initialization, whereas the system is much more robust if HGF dynamics are incorporated at $T \geq 2$. Since we hypothesize that a time delay does occur between tumor initiation and formation of the HGF feedback loop, we present results of simulations when the HGF dynamic is initialized at $T \geq 2$.

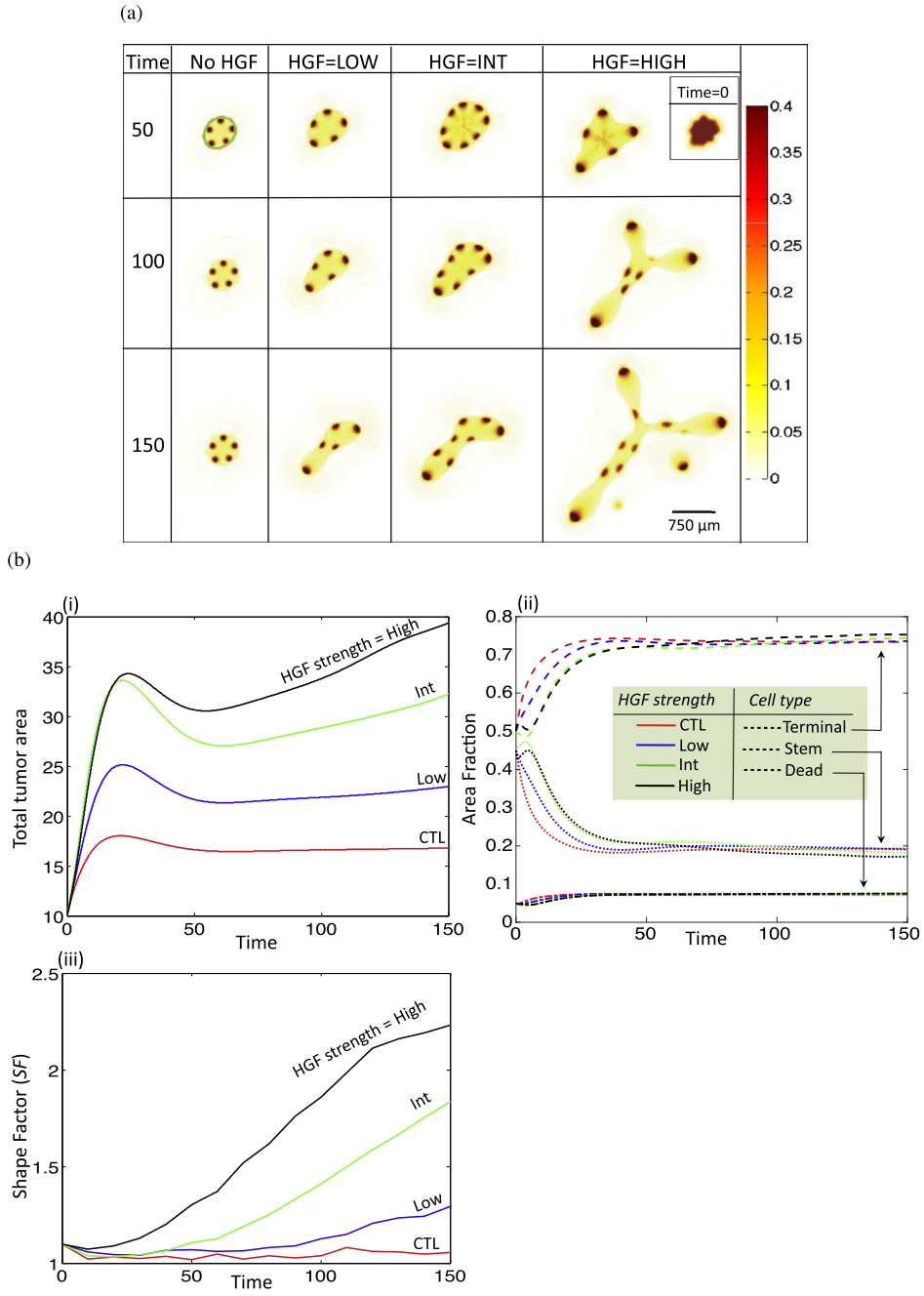

Fig. 2. HGF feedback increases tumor growth rates and enhances invasiveness. (a) Stem cell fractions for increasing HGF dynamics and $T = 50, 100, 150$. Inset in top right corner shows initial tumor shape via visualization of the stem cell fraction for all HGF dynamics at $T = 0$. (b) Area, area fraction, and shape factor. (i) Total area and (ii) area fraction for no (red), low (blue), int (green) and high (black) HGF. Area fraction is shown for different cell types: terminal, dash; stem, dot; dead, dash-dot). (iii) Shape factor (*SF*) results for the four treatment types. (For interpretation of the references to color in this figure legend, the reader is referred to the web version of this article.)

whereas the different cell fractions remain similar over all HGF strengths (Fig. 2(b)(ii)). Indeed, it has been observed that cancer stem cells constitute a stable fraction of the tumor population (Dalerba et al., 2007). In order to measure the changes in morphology induced by HGF dynamics, we consider the shape factor, *SF*, for an object, which is calculated by

$$SF(P, A) = P^2/(4\pi A), \tag{32}$$

where P and A are the object perimeter and area, respectively. The shape factor for a circle is $SF = 1$, and increases as the shape of the object deviates from a circle. The shape factor tends to increase over time in all cases, but increases more drastically as HGF dynamics increase (Fig. 2(b)(iii)), supporting the experimental results that HGF can induce branching and invasive morphology in exposed tissues and tumors, respectively (Brinkmann et al., 1995; Ikari et al., 2003; Wong et al., 2000).

We fix $T = 100$ in order to more closely observe other variables associated with the simulations, namely concentrations of c-Met, HGF, and SGF (Fig. 3(a)) and total tumor, terminal cell, and dead cell fractions (Fig. 3(b)). c-Met levels in the spots increase with increasing HGF dynamics, and there is an increase in HGF concentration at the tumor-host boundary and SGF concentration within the tumor (Fig. 3(a)). A large fraction of all the cases contain terminal cells, with a smaller co-localized percentage of dead cells, and

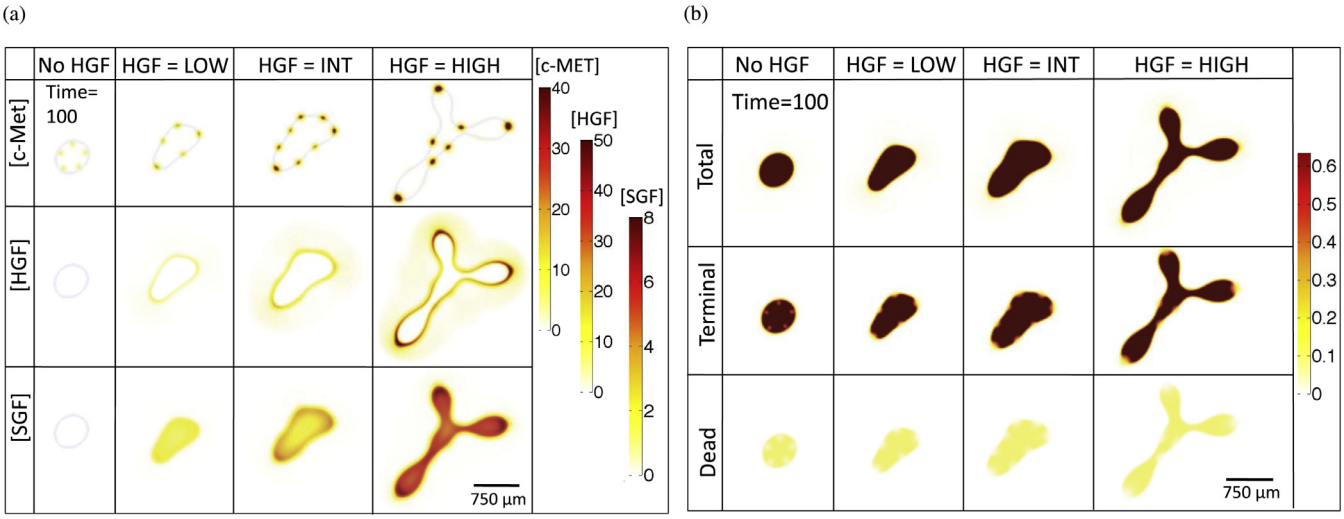

Fig. 3. Chemical species (a) and cell species (b) concentrations for increasing HGF dynamics at $T = 100$.

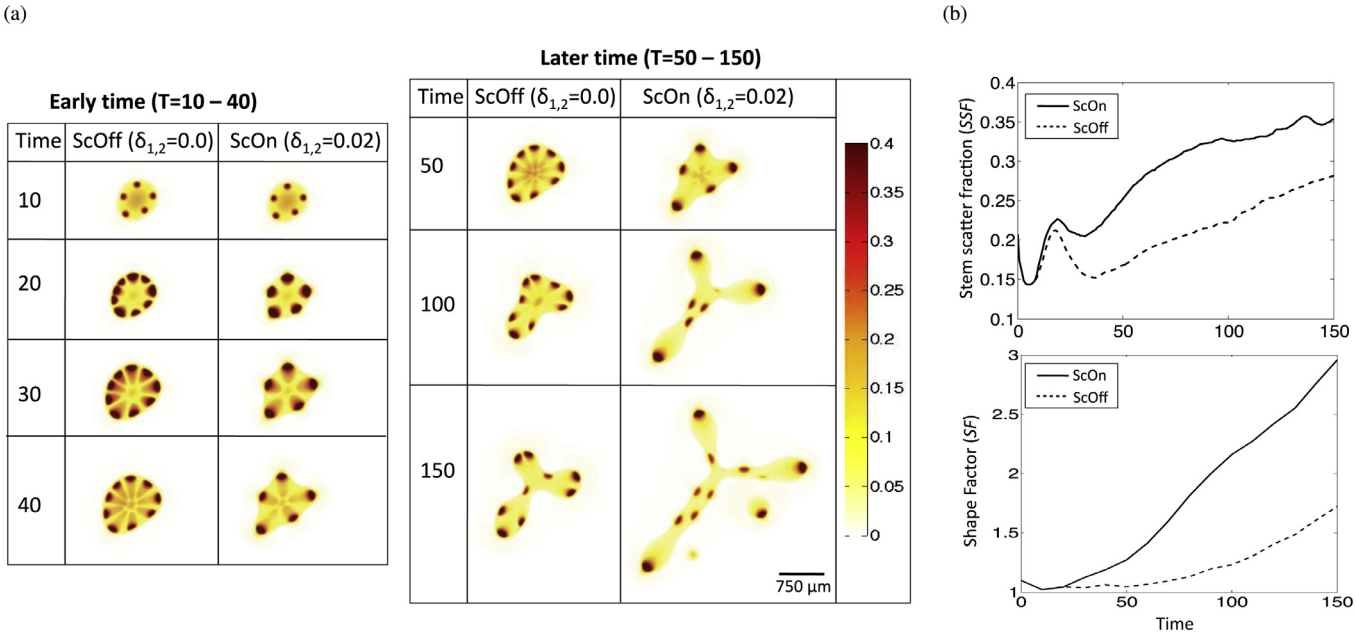

Fig. 4. Effect of c-Met-mediated cell scatter on spot formation, tumor growth, and invasive morphology in high HGF conditions. (a) Stem cell distributions in HGF high conditions and without (ScOff, $\delta_{1,2} = 0.0$) or with (ScOn, $\delta_{1,2} = 0.02$) HGF-induced effect on cell scatter. (b) Quantification of stem scatter fraction (*SSF*) and shape factor (*SF*) for ScOff and ScOn simulations. Time-course data was smoothed using Moving Average Filtering in Matlab R2014b.

with both cell types concentrated outside of the areas with stem cell spots (Fig. 3(b)).

3.2. HGF, cell scatter, and pattern formation

In order to better understand how HGF dynamics influence spot formation, we examine the early and late-time dynamics of the simulations with and without c-Met-induced cell scatter (the latter case is simulated by setting $\delta_{1,2} = 0$ in Eqs. (5) and (6)). For brevity, we call the case with $\delta_{1,2} = 0$, 'ScOff', and the case with $\delta_{1,2} = 0.02$, 'ScOn'. The values for $\delta_{1,2}$ were chosen to simulate a moderate, but observable effect, of HGF on cell-cell and cell-ECM interactions. We observe that c-Met-induced cell scatter results in loss of stem cell spots and an increase in invasive fingering (Fig. 4(a)). We can quantify these effects by measuring the shape factor (*SF*, Eq. (32)) and the stem scatter fraction (*SSF*) of the ScOn and ScOff simulations during the simulation runtime. We calculate the *SSF* by first measuring the concentration of stem cells in the host tissue, which is taken to be the area of stem cells in the host region normalized to the area of stem cells in the entire domain,

$$SSF(\phi_{SC}, \phi_T, \Omega) = \frac{\int_\Omega \phi_{SC}(1-\phi_T)dx}{\int_\Omega \phi_{SC}dx}. \tag{33}$$

We find *SSF* and *SF* are increased for the ScOn compared to the ScOff case (Fig. 4). This increase in *SSF* is due to the increased cell scatter, whereas the increase in *SF* is due to the increased heterogeneity of cell types and behavior at the tumor-host boundary.

Pattern formation is also impacted by the respective strengths of $\lambda_{1,2_{HGF}}$ in Eqs. (18), (20), and (21). In Fig. 5, we observe that if $\lambda_{1_{HGF}} = 0$, then as $\lambda_{2_{HGF}}$ increases, we eventually see a continuous strip of stem cells at the tumor host boundary. Alternatively, setting $\lambda_{2_{HGF}} = 0$ and increasing $\lambda_{1_{HGF}}$ does not result in the increase in spot number, but each spot is bigger, has higher c-Met

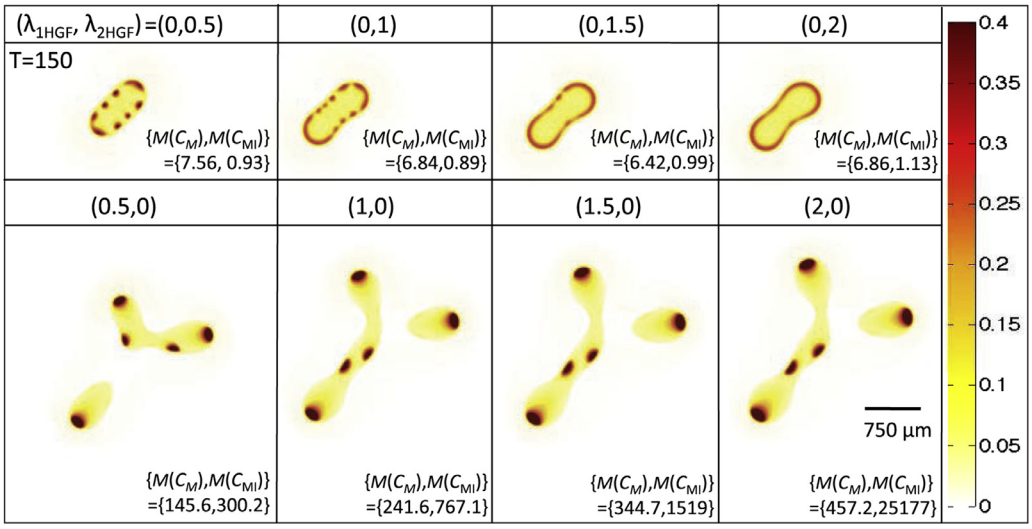

Fig. 5. Isolating the effects of $\lambda_{1_{HGF}}$ and $\lambda_{2_{HGF}}$ in Eqs. (18), (20), and (21) on stem cell distributions and concentrations of c-Met and c-Met inhibitors. Stem cell distribution is shown for $T = 150$ and $(\lambda_{1_{HGF}}, \lambda_{2_{HGF}})$ as indicated. The bottom right-hand corner of each simulation shows the maximum concentration of c-Met and c-Met inhibitor that is reached (the short-hand $M(X) = \max(X)$ is used). Note that δ_1 and δ_2 in Eqs. (5) and (6) are set to 0 to control for the HGF-induced effect on cell scatter.

and c-Met inhibitor concentrations, and gives rise to larger tumor fingers.

To obtain an analytical understanding of the effect of HGF action with respect to these two parameters, we performed a Turing Analysis on a reduced system of two equations modeling a nonlinear reaction-diffusion system with a forcing term (Appendix A). In the reduced system (A.1), we find that an increase in the term ν_a, which is linearly proportional to $\lambda_{1_{HGF}} C_{HGF}$, results in increased steady state $\bar{a}$ and $\bar{b}$, which correspond to C_M and C_{MI}, respectively, in the original system, and no effect on the critical wavenumber, q_{min}, (Eq. (A.6)) or maximum eigenvalues (Eq. (A.8)) of A_q, as defined in Eq. (A.7). This system corresponds to the simulations with $(\lambda_{1_{HGF}}, \lambda_{2_{HGF}}) = (x, 0)$, where x is positive, as shown in the bottom row of Fig. 5, where we indeed see no change in the number of stem cell spots, but do see an increase in both C_M and C_{MI}. Alternatively, the Turing Analysis on system (A.9) shows that increasing the term E_a, which corresponds to $\lambda_{2_{HGF}} C_{HGF}$ in the original system, leads to a decrease in the critical wavenumber q_{min} and maximal eigenvalues of A_q (Fig. A.1). We would expect such a system to eventually become more stable with increasing E_a, especially at low ν_a, since the decrease in maximal eigenvalues indicates that the growth rates of the perturbations will decrease with increasing E_a. Although q_{min} is decreasing, which signals that we may find more unstable wave numbers, a very low perturbation growth rate suggests that pattern formation will not occur. In the original system, when we take $(\lambda_{1_{HGF}}, \lambda_{2_{HGF}}) = (0, x)$, with x positive, we indeed see a uniform band of stem cells forming when $\lambda_{2_{HGF}}$ is large enough (Fig. 5).

3.3. Effect of negative feedback on tumor growth

A common characteristic of tumors that progress from preneoplastic lesions to neoplasms is that they lose the ability to respond to negative growth feedback signals (Hanahan and Weinberg, 2011). For example, in colorectal cancer, resistance to TGFβ by mutation of a cognate receptor is associated with progression from adenoma to malignant carcinoma (Grady et al., 1998). The TGFβ pathway can also be inactivated by a mutation of the TGFβ receptor TGFβR2 or by inactivation of downstream signaling components SMAD2, SMAD3, or SMAD4 (Markowitz and Bertagnolli, 2009).

Loss of response to members of the TGFβ family is correlated with poorer prognosis in a clinical setting (Pickup et al., 2013). Therefore, to model the effect of HGF dynamics in a tumor that has progressed beyond the initial stages, we reduce the strength of TGFβ feedback on stem cell self-renewal from $\psi_0 = 1.0$ to $\psi_0 = 0.5$. When compared to the case with $\psi_0 = 1.0$, the simulation results with reduced response to negative feedback have a greater total area and shape factor, indicating the enhanced invasive potential of such tumors (Fig. 6).

3.4. Therapy

Therapies targeting various aspects of the HGF/c-Met axis, including antibodies against HGF and c-Met, HGF-competitive analogs, tyrosine kinase inhibitors (TKIs) targeting c-Met, and downstream pathway inhibitors are currently in development (Blumenschein et al., 2012; Knudsen and Vande Woude, 2008). Over 20 drugs are currently in Phase I-III clinical trials (Cecchi et al., 2012), indicating strong interest by the biomedical community in translating the accumulated knowledge of the HGF/c-Met axis into cancer therapeutics. We model targeted therapy by changing ν_0, the strength of c-Met auto-activation, and $\lambda_{1,2_{HGF}}$, the strength of HGF-induced c-Met activation, in Eqs. (20) and (21). Lowering $\lambda_{1_{HGF}}$ and $\lambda_{2_{HGF}}$ models drugs that act by inhibiting HGF (class T_1), while lowering ν_0 represents drugs that specifically disrupt c-Met auto-catalysis. Drugs that inhibit c-Met or its downstream effectors lower both auto-catalysis rates and the ability of HGF to upregulate c-Met products (class T_2). Therefore, activity of such drugs should be modeled by lowering all three parameters. We model class T_1 and T_2 drugs as follows, at $T = 50$ we apply either therapy T_1, which lowers $\lambda_{1_{HGF}}$ and $\lambda_{2_{HGF}}$ from 0.5 to 0.05 or therapy T_2, which lowers $\lambda_{1_{HGF}}$ and $\lambda_{2_{HGF}}$ to 0.005 and ν_0 from 1.0 to 0.1 (Fig. 7). We choose these two therapies as they represent two different classes of drugs as described above, and they also represent the two classes of therapy results that were observed when both parameters were systematically lowered for high HGF (Figure S2). Therapy is applied until the last time point, $T = 150$. We find that therapy class T_1 results in decreased total area and shape factor, but it is the T_2 class that results in a shape factor close to 1, indicating that the invasive morphology has been significantly reduced along with total tumor size. It has been shown that very strong inhibition of

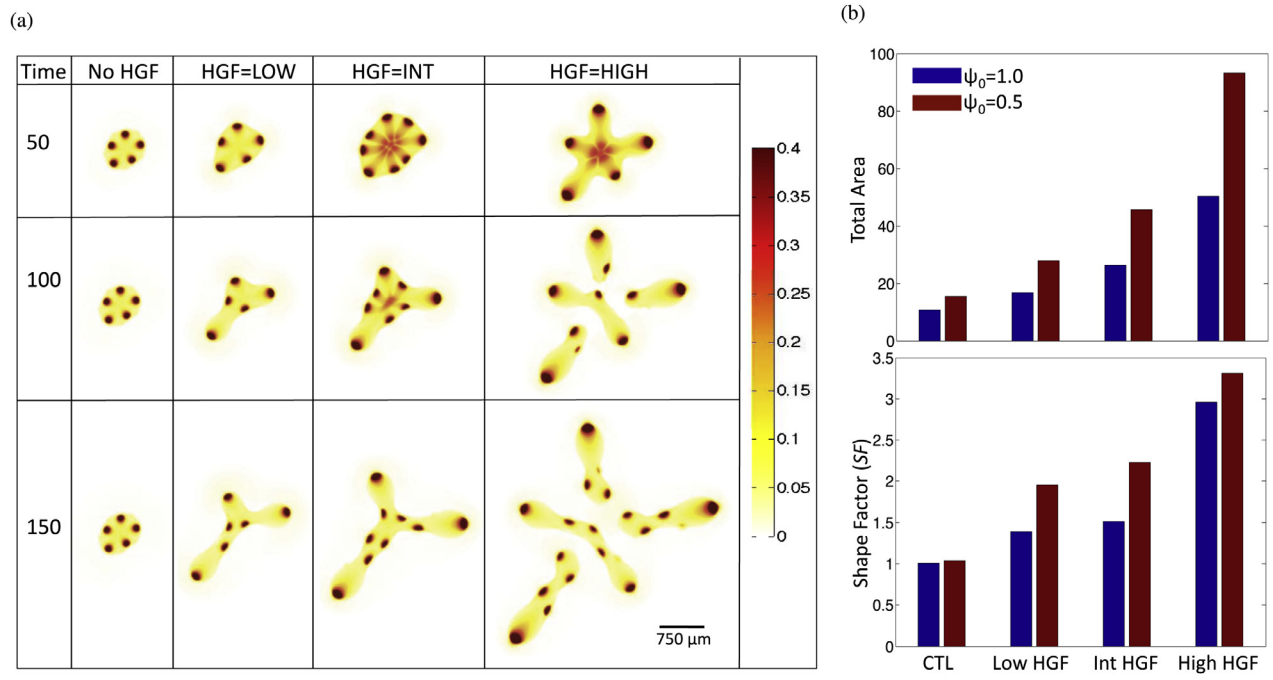

Fig. 6. Tumor evolution under decreased negative feedback. From the baseline simulation, ψ_0 in Eq. (13) is lowered from 1.0 to 0.5. (a) Stem cell distributions for increasing HGF dynamics. (b) Comparison of total area (top panel) and shape factor (*SF*) (bottom panel) between $\psi_0 = 1$ (blue) and $\psi_0 = 0.5$ (red) simulations at $T = 150$. (For interpretation of the references to color in this figure legend, the reader is referred to the web version of this article.)

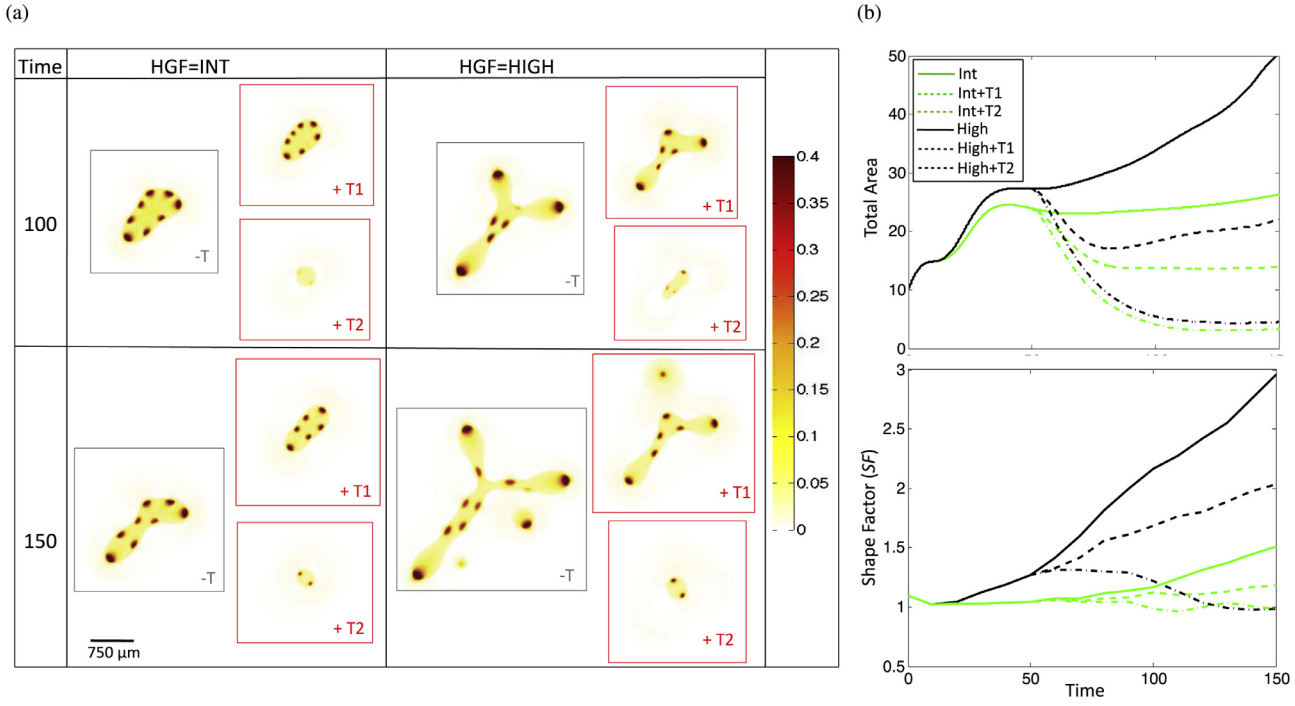

Fig. 7. Response of tumor to anti-HGF (T_1, $\lambda_{1_{HGF}}$ and $\lambda_{2_{HGF}}$ lowered from 0.5 to 0.05) and anti-c-Met (T_2, $\lambda_{1_{HGF}}$ and $\lambda_{2_{HGF}}$ lowered from 0.5 to 0.005 and ν_0 lowered from 1.0 to 0.1) therapy applied at $T = 50$. (a) Representative stem cell fraction and (b) total area and shape factor for no therapy, T_1, and T_2 applied to int and high HGF tumors.

c-Met phosphorylation ($>90\%$) is required for significant inhibition of tumor growth ($>50\%$) in a tumor xenograft mouse model (Yamazaki et al., 2008), which is consistent with our simulation results. Additionally, we find that when therapy is terminated prematurely, the tumor grows back rapidly (Figure S2), indicating that ultimate tumor eradication requires combination therapy and/or surgical resection alongside anti-HGF/c-Met drugs. We note that in Yamazaki et al. (2008), mice were euthanized maximally 24 h after the last therapy dose, which lasted between 9–11 days, hence it is not known what the tumor behavior would have been for a longer period after therapy cessation.

4. Discussion

By incorporating tumor-produced SGF and the HGF/c-Met axis into a multispecies model of tumor growth, we have shown that

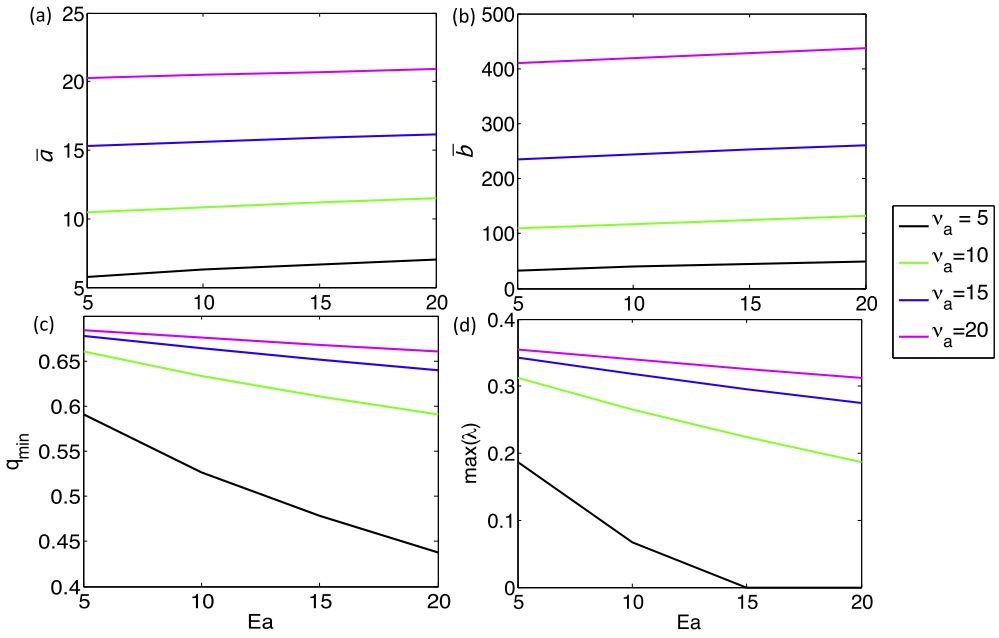

Fig. A1. Effect of increasing ν_a and E_a in System (A.1) on (a) $\bar{a}$, (b) $\bar{b}$, (c) q_{min}, and (d) $\max(\lambda)$, where $\bar{a}$ and $\bar{b}$ give stationary states for the system without diffusion, q_{min} is the critical wavenumber for the system, and $\max(\lambda)$ is the maximum eigenvalue of A_q, where A_q is taken as in Eq. (A.7) with $q = q_{min}$.

establishment of a dynamic interaction between the tumor and its microenvironment results in increased tumor growth and morphological instability, the latter due in part to increased cell-species heterogeneity at the tumor-host boundary. Indeed, such a phenomenon has been investigated by Cristini et al. (2005). Using both experimental and simulation results, (Cristini et al., 2005) showed that spatially heterogeneous cell proliferation, alongside disruption of cell-cell adhesion, results in invasive fingering and migration of cell clusters. In their model, the heterogeneity occurred due to heterogeneous distribution of oxygen, nutrients, and pH levels caused by atypical tumor vasculature and other disruptions to diffusion in the tumor. Similarly, in a hybrid cellular automata and PDE tumor growth model, (Sottoriva et al., 2010) showed that a tumor that has a 100% CSC fraction yields a sphere-like morphology whereas tumors with low CSC fractions (in this model, CSCs differ from differentiated cells, DCs, in that CSCs have unlimited replicative potential, can migrate and mutate unlike the DCs), show invasive fingering with highly irregular shape. In our model, the heterogeneity occurs due to formation of stem cell spots at the tumor-host boundary via a Turing mechanism of c-Met and c-Met inhibitors. This heterogeneity is exacerbated by the presence of HGF-SGF signaling cross-talk since the effect of HGF on cell scatter results in a more irregular spot distribution at the tumor-host boundary, and the effect of HGF on proliferation/self-renewal increases the size of the remaining spots. Thus, when the effect of HGF on cell scatter is removed from the model, the tumor becomes more stable due to a more uniform distribution of stem cell spots at the tumor-host boundary, even though there are more such spots than in the original model (Fig. 4). (Cristini et al., 2005) propose that suppression of morphologic instability via homogenization of cell proliferation and increase in cell-cell adhesion will result in a more compact, noninvasive tumor morphology. Our therapy results support their conclusions: when we block the HGF/c-Met axis sufficiently enough to reduce the highly proliferative spot size, the tumor does not only grow more slowly, but it grows in a more compact manner (Fig. 7).

We find that invasive behavior is further increased if the tumor lowers responsiveness to tumor-derived pro-differentiation signals, which is a traditional hallmark of neoplastic development (Hanahan and Weinberg, 2000). We have not addressed a portion of the pleiotropic effects of TGFβ that constitute the 'TGFβ paradox'. Namely, our model does not consider that in certain cases, TGFβ can increase cellular motility, as well as hasten the Epithelial-to-Mesenchymal Transition (EMT) of tumorigenic epithelial cells (Pickup et al., 2013). Moreover, it has been found that in advanced cancers, immune components and fibroblasts can produce TGFβ, which has tumor-promoting effects (Massagué, 2008). In this study, we only model the anti-proliferative effects of TGFβ, with its production localized to terminal cells. Incorporation of the tumor-promoting action of TGFβ may be best done using a specific cancer model and data, since such effects show greater diversity among different cancers than the other growth factors modeled in this study.

By modeling anti-HGF and anti-c-Met therapy, we show how disruption of the HGF/c-Met cascade can lower tumor invasiveness and growth, thereby providing theoretical evidence that targeting tumor-microenvironment dynamics is a promising avenue for therapeutic development. An important consideration in clinical development of anti-HGF/c-Met therapies is patient selection and stratification. Studies on efficacy of HGF/c-Met targeted therapies have consistently shown that patients with high c-Met expression levels respond best to these therapies (Graveel et al., 2013), indicating that patient pre-selection based on tumor biomarkers of HGF/c-Met axis activation can improve therapy outcomes (Blumenschein et al., 2012). As our model assumes c-Met as a main driver in stem cell self-renewal and division rate, it is most directly applicable to patients with high c-Met activity.

Many of our assumptions and results are based upon quantification of specific features of the tumor and its microenvironment, including the spatially-distributed stem cell fraction of the tumor, and chemical diffusion, uptake, and activity coefficients. In order to better align our model with experimental observations, it is necessary to use an experimental system that is capable of recapitulating and capturing some of the complexities of the tumor microenvironment. In their review of emerging technologies in this field, (Guldner and Zhang, 2015) noted that new technology is nec-

essary to explore the tumor microenvironment that incorporates spatial and temporal dynamics of tumor-microenvironmental interactions, and can measure cell-type specific behavior. They discuss emerging technologies that can aide in this goal, including deep tissue optical sectioning, intravital microscopy (IVM, the imaging of live animal tissue), and *in situ* cell-type specific genetic isolation. For example, Tanaka et al. (2012) used IVM in a liver metastatic xenograft system where RFP-labeled human colorectal cells were injected into GFP-expressing nude mice to obtain a time-series of the phenotypic changes in tumor and host during liver metastasis and with and without chemotherapy. In addition, development of sophisticated 3D-culture systems where protein and drug diffusion and uptake rates can be measured via techniques such as FRAP or FLIM-FRET, which are already in use (Conway et al., 2014; Talukdar and Kundu, 2012). Therefore, it is possible to construct an appropriate experimental system to test the hypotheses generated by our model regarding quantifiable tumor behavior with an activated HGF/c-Met axis, such as increased invasiveness and formation of areas with high stem-cell concentration at the tumor-host boundary.

Acknowledgements

This work was supported in part by the National Science Foundation Division of Mathematical Sciences (JSL), Grant P50GM76516 for the Center of Excellence in Systems Biology at the University of California, Irvine, P30CA062203 for the Chao Family Comprehensive Cancer Center at University of California, Irvine, and predoctoral Training Grants T32EB009418 from the National Institute of Biomedical Imaging and Bioengineering and T32HD060555 from the Eunice Kennedy Shriver National Instituteof Health and Human Development (AK). The authors would also like to thank the reviewers for their constructive comments and suggestions.

Appendix A. Turing analysis of nonlinear activator-inhibitor dynamics with additional forcing term

A1. Simplifed nonlinear activator-inhibitor model

In Eqs. (18)–(22) (nondimensionalized in Eqs. (27)–(31)), we model the effect of HGF on c-Met activation using two parameters, $\lambda_{1_{HGF}}$ and $\lambda_{2_{HGF}}$. To better understand how each parameter affects pattern formation, we develop a simplified nonlinear model of activator-inhibitor dynamics and perform a Turing analysis on it. We begin with the system

$$\begin{aligned} \dot{a} &= \nu_a \frac{a^2}{b} - d_a a + D_a \frac{\partial^2 a}{\partial x^2}, \\ \dot{b} &= \nu_b a^2 - d_b b + D_b \frac{\partial^2 b}{\partial x^2}, \end{aligned} \tag{A.1}$$

where a is the activator and b is the inhibitor, ν_a and ν_b are the respective production rates of a and b, and d_a and d_b are the respective decay rates of a and b. This system represents $\lambda_{2_{HGF}} = 0$ and ν_a as linearly proportional to $\lambda_{1_{HGF}} C_{HGF}$. Taking $f_1(a,b) = \nu_a \frac{a^2}{b} - d_a a$ and $f_2(a,b) = \nu_b a^2 - d_b b$, we find a stationary state without diffusion for (A.1), i.e. we identify $(a,b) = (\bar{a},\bar{b})$ such that $(f_1, f_2) = (0,0)$. There is one solution,

$$(\bar{a},\bar{b}) = \left(\frac{d_b \nu_a}{d_a \nu_b}, \frac{d_b \nu_a^2}{d_a^2 \nu_b} \right). \tag{A.2}$$

We note that $\bar{a}$ is proportional to ν_a. Thus, we expect that if $\lambda_{2_{HGF}}$ is negligible in the original system, then an increase in $\lambda_{1_{HGF}}$ should result in higher steady state c-Met concentration.

In order to simplify stability analysis of the system, we take $D_a = 1$ and $D_b = 25$, analogous to nondimensionalized values for the parameters D_M and D_{MI}, respectively. The Jacobian of the system is

$$J = (J_{ij}) = \frac{\partial f_i}{\partial u_j} = \begin{bmatrix} \frac{2a\nu_a}{b} - d_b & -\nu_a^2/b^2 \\ 2\nu_b a & -d_b \end{bmatrix}. \tag{A.3}$$

Then, taking $A = (a_{ij}) = J|_{\bar{a},\bar{b}}$, we have

$$A = (a_{ij}) = \begin{bmatrix} d_a & \frac{-d_a^2}{\nu_a} \\ \frac{2d_b\nu_a}{d_a} & -d_b \end{bmatrix}. \tag{A.4}$$

In order for a and b to be stable in the absence of diffusion, we must have

- $a_{11} + a_{22} < 0$,
- $a_{11}a_{22} - a_{12}a_{21} > 0$,

which occurs if $d_a - d_b < 0$ and $-d_a d_b + 2d_a d_b = d_a d_b > 0$. Diffusion will destabilize the system when the wavenumber, q, is near

$$q_{min}^2 = \frac{1}{2}\left(\frac{a_{22}}{D_2} + \frac{a_{11}}{D_1} \right). \tag{A.5}$$

In our case, we obtain

$$q_{min} = \sqrt{\frac{1}{2}\left(\frac{-d_b}{25} + d_a \right)} \tag{A.6}$$

We find that q_{min} does not depend on ν_a. Moreover, the growth rate of perturbations to the steady state is given by the eigenvalues of the matrix

$$A_q = \begin{bmatrix} a_{11} - D_1 q^2 & a_{12} \\ a_{21} & a_{22} - D_2 q^2 \end{bmatrix}. \tag{A.7}$$

The eigenvalues of A_q are

$$\begin{aligned} \lambda_{1,2} = \frac{1}{2}\Big(& d_a - d_b - 26q^2 \\ & \pm \sqrt{d_a^2 - 6d_a d_b + d_b^2 + 48 d_a q^2 + 48 d_b q^2 + 576 q^4} \Big). \end{aligned} \tag{A.8}$$

Importantly, the eigenvalues also do not depend on ν_a.

We can thus conclude that in an activator-inhibitor reaction of this type, the steady state of a will be directly proportional to ν_a, but pattern formation will not be influenced.

A2. Simplified nonlinear activator-inhibitor model with an additional forcing term

We now introduce the additional term E_a to system (A.1) to represent non-trivial $\lambda_{2_{HGF}}$ as follows:

$$\begin{aligned} \dot{a} &= \nu_a \frac{a^2 + E_a}{b} - d_a a + D_a \frac{\partial^2 a}{\partial x^2}, \\ \dot{b} &= \nu_b a^2 - d_b b + D_b \frac{\partial^2 b}{\partial x^2}. \end{aligned} \tag{A.9}$$

Taking $f_1(a,b) = \nu_a \frac{a^2+E_a}{b} - d_a a$ and $f_2(a,b) = \nu_b a^2 - d_b b$, there is one real solution to the system $(f_1, f_2) = (0,0)$, but it is unwieldy analytically. Therefore, we find $(\bar{a},\bar{b})$, A, q_{min}, and eiqenvalues of A_q for specific values of ν_a and E_a. We take $\nu_a = \{5, 10, 15, 20\}$ and $E_a = \{5, 10, 15, 20\}$. We also take $d_a = d_b = \nu_b = 1$. We find the real-valued $(\bar{a},\bar{b})$ using the 'solve' function in Matlab for $(f_1, f_2) = (0,0)$.

In Fig. A.1(a,b), we observe that while increasing ν_a leads to an increase in both $\bar{a}$ and $\bar{b}$, the effect of E_a on $\bar{a}$ and $\bar{b}$ is much less pronounced.

As before, we find $A = (a_{ij})$, the Jacobian of the system $(f_1(a, b), f_2(a, b))$ at $(\bar{a}, \bar{b})$ and $\nu_b = d_a = d_b = 1$,

$$A = \begin{bmatrix} \frac{2\nu_a \bar{a}}{b} - 1 & -\frac{\nu_a(a^2 + E_a)}{\bar{b}^2} \\ 2a & -1 \end{bmatrix} \tag{A.10}$$

We note that for the values of ν_a and E_a considered, the conditions for stability of the system without diffusion $(^*)$ are satisfied.

We use Eq. (A.5) to calculate q_{min} for discrete values of ν_a and E_a (Fig. A.1c). We note that q_{min} decreases as E_a increases, and this decrease is stronger at lower values of ν_a. Moreover, taking A_q as in Eq. (A.7), with $q = q_{min}$, the maximum eigenvalue decreases with increasing E_a and decreasing ν_a (Fig. A.1(d)).

Supplementary material

Supplementary material associated with this article can be found, in the online version, at 10.1016/j.jtbi.2017.11.025.

References

Anderson, A.R.A., Weaver, A.M., Cummings, P.T., Quaranta, V., 2006. Tumor morphology and phenotypic evolution driven by selective pressure from the microenvironment. Cell 127 (5), 905–915. doi:10.1016/j.cell.2006.09.042.

Bhowmick, N.A., Neilson, E.G., Moses, H.L., 2004. Stromal fibroblasts in cancer initiation and progression. Nature 432 (7015), 332–337. doi:10.1038/nature03096.

Birchmeier, C., Birchmeier, W., Gherardi, E., Vande Woude, G.F., 2003. Met, metastasis, motility and more. Nat. Rev. Mol. Cell Biol. 4 (12), 915–925. doi:10.1038/nrm1261.

Blumenschein, G.R.Jr, Mills, G.B., Gonzalez-Angulo, A.M., 2012. Targeting the hepatocyte growth factor-cmet axis in cancer therapy. J. Clin. Oncol. 30 (26), 3287–3296. doi:10.1200/JCO.2011.40.3774.

Brinkmann, V., Foroutan, H., Sachs, M., Weidner, K., Birchmeier, W., 1995. Hepatocyte growth factor/scatter factor induces a variety of tissue-specific morphogenic progrmas in epithelial cells. J. Cell Biol. 131 (6 Pt 1), 1573–1586.

Byrne, H.M., 2010. Dissecting cancer through mathematics: from the cell to the animal model. Nat. Rev. Cancer. 10 (3), 221–230. doi:10.1038/nrc2808.

Cecchi, F., Rabe, D.C., Bottaro, D.P., 2012. Targeting the hgf/met signaling pathway in cancer therapy. Expert Opin. Ther. Targets 16 (6), 553–572. doi:10.1517/14728222.2012.680957.

Christensen, J.G., Burrows, J., Salgia, R., 2005. c-met as a target for human cancer and characterization of inhibitors for therapeutic intervention. Cancer Lett. 225 (1), 1–26. doi:10.1016/j.canlet.2004.09.044.

Conway, J.R.W., Carragher, N.O., Timpson, P., 2014. Developments in preclinical cancer imaging: innovating the discovery of therapeutics. Nat Rev Cancer 14 (5), 314–328. doi:10.1038/nrc3724.

Cristini, V., Frieboes, H.B., Gatenby, R., Caserta, S., Ferrari, M., Sinek, J., 2005. Morphologic instability and cancer invasion. Clin. Cancer Res. 11 (19 Pt 1), 6772–6779. doi:10.1158/1078-0432.CCR-05-0852.

Dale, L., Wardle, F.C., 1999. A gradient of bmp activity specifies dorsal-ventral fates in early xenopus embryos. Semin. Cell Dev. Biol. 10 (3), 319–326. doi:10.1006/scdb.1999.0308.

Dalerba, P., Cho, R.W., Clarke, M.F., 2007. Cancer stem cells: models and concepts. Annu. Rev. Med. 58, 267–384. doi:10.1146/annurev.med.58.062105.204854.

De Luca, A., Gallo, M., Aldinucci, D., Ribatti, D., Lamura, L., D'Alessio, A., De Filippi, R., Pinto, A., Normanno, N., 2010. The role of the egfr ligand/receptor system in the secretion of angiogenic factors in mesenchymal stem cells.. J. Cell Physiol. doi:10.1002/jcp.22548.

Deisboeck, T.S., Wang, Z., Macklin, P., Cristini, V., 2011. Multiscale cancer modeling. Annu. Rev. Biomed. Eng. 13, 127–155. doi:10.1146/annurev-bioeng-071910-124729.

Duffy, M.J., 2004. The urokinase plasminogen activator system: role in malignancy. Curr. Pharm. Des. 10 (1), 39–49.

Eftimie, R., Bramson, J.L., Earn, D.J.D., 2011. Interactions between the immune system and cancer: a brief review of non-spatial mathematical models. Bull. Math. Biol. 73 (1), 2–32. doi:10.1007/s11538-010-9526-3.

Eikenberry, S., Thalhauser, C., Kuang, Y., 2009. Tumor-immune interaction, surgical treatment, and cancer recurrence in a mathematical model of melanoma. PLoS Comput. Biol. 5 (4), e1000362. doi:10.1371/journal.pcbi.1000362.

Frank, S., 2007. Dynamics of Cancer: Incidence, Inheritence, and Evolution. Princeton University Press.

Frieboes, H.B., Wu, M., Lowengrub, J., Decuzzi, P., Cristini, V., 2013. A computational model for predicting nanoparticle accumulation in tumor vasculature. PLoS One 8 (2), e56876. doi:10.1371/journal.pone.0056876.

Frieboes, H.B., Zheng, X., Sun, C.-H., Tromberg, B., Gatenby, R., Cristini, V., 2006. An integrated computational/experimental model of tumor invasion. Cancer Res. 66 (3), 1597–1604. doi:10.1158/0008-5472.CAN-05-3166.

Friedl, P., Wolf, K., 2008. Tube travel: the role of proteases in individual and collective cancer cell invasion. Cancer Res. 68 (18), 7247–7249. doi:10.1158/0008-5472.CAN-08-0784.

Gierer, A., Meinhardt, H., 1972. A theory of biological pattern formation. Kybernetik 12 (1), 30–39.

Gohda, E., Matsunaga, T., Kataoka, H., Takebe, T., Yamamoto, I., 1994. Induction of hepatocyte growth factor in human skin fibroblasts by epidermal growth factor, platelet-derived growth factor and fibroblast growth factor. Cytokine 6 (6), 633–640.

Gohda, E., Matsunaga, T., Kataoka, H., Yamamoto, I., 1992. Tgf-beta is a potent inhibitor of hepatocyte growth factor secretion by human fibroblasts. Cell Biol. Int. Rep. 16 (9), 917–926.

Grady, W.M., Rajput, A., Myeroff, L., Liu, D.F., Kwon, K., Willis, J., Markowitz, S., 1998. Mutation of the type ii transforming growth factor-beta receptor is coincident with the transformation of human colon adenomas to malignant carcinomas. Cancer Res. 58 (14), 3101–3104.

Graveel, C.R., Tolbert, D., Vande Woude, G.F., 2013. Met: a critical player in tumorigenesis and therapeutic target. Cold Spring Harb. Perspect. Biol. 5 (7). doi:10.1101/cshperspect.a009209.

Guldner, I.H., Zhang, S., 2015. A journey to uncharted territory: new technical frontiers in studying tumor-stromal cell interactions. Integr. Biol. (Camb.) 7 (2), 153–161. doi:10.1039/c4ib00192c.

Hanahan, D., Coussens, L.M., 2012. Accessories to the crime: functions of cells recruited to the tumor microenvironment. Cancer Cell 21 (3), 309–322. doi:10.1016/j.ccr.2012.02.022.

Hanahan, D., Weinberg, R., 2000. The hallmarks of cancer. Cell 100 (1), 57–70.

Hanahan, D., Weinberg, R.A., 2011. Hallmarks of cancer: the next generation. Cell 144 (5), 646–674. doi:10.1016/j.cell.2011.02.013.

Harrison, P., Bradley, L., Bomford, A., 2000. Mechanism of regulation of hgf/sf gene expression in fibroblasts by tgf-beta1. Biochem. Biophys. Res. Commun. 271 (1), 203–211. doi:10.1006/bbrc.2000.2612.

Huang, S.S., Huang, J.S., 2005. Tgf-beta control of cell proliferation. J. Cell Biochem. 96 (3), 447–462. doi:10.1002/jcb.20558.

Ikari, T., Hiraki, A., Seki, K., Sugiura, T., Matsumoto, K., Shirasuna, K., 2003. Involvement of hepatocyte growth factor in branching morphogenesis of murine salivary gland. Dev. Dyn. 228 (2), 173–184.

Jeffers, M., Rong, S., Vande Woude, G.F., 1996. Enhanced tumorigenicity and invasion-metastasis by hepatocyte growth factor/scatter factor-met signalling in human cells concomitant with induction of the urokinase proteolysis network. Mol. Cell Biol. 16 (3), 1115–1125.

Jones, C.M., Armes, N., Smith, J.C., 1996. Signalling by tgf-beta family members: short-range effects of xnr-2 and bmp-4 contrast with the long-range effects of activin. Curr. Biol. 6 (11), 1468–1475.

Jones, C.M., Smith, J.C., 1998. Establishment of a bmp-4 morphogen gradient by long-range inhibition. Dev. Biol. 194 (1), 12–17. doi:10.1006/dbio.1997.8752.

Joo, K.M., Jin, J., Kim, E., Ho Kim, K., Kim, Y., Gu Kang, B., Kang, Y.-J., Lathia, J.D., Cheong, K.H., Song, P.H., Kim, H., Seol, H.J., Kong, D.-S., Lee, J.-I., Rich, J.N., Lee, J., Nam, D.-H., 2012. Met signaling regulates glioblastoma stem cells. Cancer Res 72 (15), 3828–3838. doi:10.1158/0008-5472.CAN-11-3760.

Jordan, C.T., Guzman, M.L., Noble, M., 2006. Cancer stem cells. N. Engl. J. Med. 355 (12), 1253–1261. doi:10.1056/NEJMra061808.

Kalluri, R., Zeisberg, M., 2006. Fibroblasts in cancer. Nat. Rev. Cancer 6 (5), 392–401. doi:10.1038/nrc1877.

Karagiannis, G.S., Poutahidis, T., Erdman, S.E., Kirsch, R., Riddell, R.H., Diamandis, E.P., 2012. Cancer-associated fibroblasts drive the progression of metastasis through both paracrine and mechanical pressure on cancer tissue. Mol. Cancer Res. 10 (11), 1403–1418. doi:10.1158/1541-7786.MCR-12-0307.

Katira, P., Bonnecaze, R.T., Zaman, M.H., 2013. Modeling the mechanics of cancer: effect of changes in cellular and extra-cellular mechanical properties. Front. Oncol. 3, 145. doi:10.3389/fonc.2013.00145.

Knudsen, B.S., Vande Woude, G., 2008. Showering c-met-dependent cancers with drugs. Curr. Opin. Genet. Dev. 18 (1), 87–96. doi:10.1016/j.gde.2008.02.001.

Konstorum, A., Sprowl, S.A., Lander, A.D., Waterman, M.L., Lowengrub, J.S., 2013a. Elaboration of a multispecies model of solid tumor growth with tumor-host interactions. Proc. 3rd Int Conf. Appl. Nonlinear Dyn. 295–303.

Konstorum, A., Sprowl, S.A., Waterman, M.L., Lander, A.D., Lowengrub, J.S., 2013b. Predicting mechanism of biphasic growth factor action on tumor growth using a multi-species model with feedback control. J. Coupled Syst. Multiscale Dyn. 1 (4), 459–467. doi:10.1166/jcsmd.2013.1028.

Kreso, A., Dick, J.E., 2014. Evolution of the cancer stem cell model. Cell Stem Cell 14 (3), 275–291. doi:10.1016/j.stem.2014.02.006.

Le Bras, G.F., Loomans, H.A., Taylor, C.J., Revetta, F.L., Andl, C.D., 2014. Activin a balance regulates epithelial invasiveness and tumorigenesis. Lab Invest. 94 (10), 1134–1146. doi:10.1038/labinvest.2014.97.

Li, M., Xin, X., Wu, T., Hua, T., Wang, H., Wang, H., 2015. Stromal cells of endometrial carcinoma promotes proliferation of epithelial cells through the hgf/c-met/akt signaling pathway. Tumour Biol. doi:10.1007/s13277-015-3309-2.

Li, Y., Li, A., Glas, M., Lal, B., Ying, M., Sang, Y., Xia, S., Trageser, D., Guerrero-Cázares, H., Eberhart, C.G., Quiñones-Hinojosa, A., Scheffler, B., Laterra, J., 2011. c-met signaling induces a reprogramming network and supports the glioblastoma stem-like phenotype. Proc. Natl. Acad. Sci. U S A 108 (24), 9951–9956. doi:10.1073/pnas.1016912108.

Lim, Y.C., Kang, H.J., Moon, J.H., 2014. C-met pathway promotes self-renewal and tumorigenecity of head and neck squamous cell carcinoma stem-like cell. Oral Oncol. 50 (7), 633–639. doi:10.1016/j.oraloncology.2014.04.004.

Lombardo, Y., Scopelliti, A., Cammareri, P., Todaro, M., Iovino, F., Ricci-Vitiani, L., Gulotta, G., Dieli, F., de Maria, R., Stassi, G., 2011. Bone morphogenetic protein 4 induces differentiation of colorectal cancer stem cells and increases their response to chemotherapy in mice. Gastroenterology 140 (1), 297–309. doi:10.1053/j.gastro.2010.10.005.

Lowengrub, J.S., Frieboes, H.B., Jin, F., Chuang, Y.-L., Li, X., Macklin, P., Wise, S.M., Cristini, V., 2010. Nonlinear modelling of cancer: bridging the gap between cells and tumours. Nonlinearity 23 (1). R1–R9

Markowitz, S.D., Bertagnolli, M.M., 2009. Molecular origins of cancer: molecular basis of colorectal cancer. N. Engl. J. Med. 361 (25), 2449–2460. doi:10.1056/NEJMra0804588.

Massagué, J., 2008. Tgfbeta in cancer. Cell 134 (2), 215–230. doi:10.1016/j.cell.2008.07.001.

Matsumoto, K., Nakamura, T., 2006. Hepatocyte growth factor and the met system as a mediator of tumor-stromal interactions.. Int. J. Cancer 119 (3), 477–483. doi:10.1002/ijc.21808.

Medema, J.P., 2013. Cancer stem cells: the challenges ahead. Nat. Cell Biol. 15 (4), 338–344. doi:10.1038/ncb2717.

Moses, H.L., Serra, R., 1996. Regulation of differentiation by tgf-beta. Curr. Opin. Genet. Dev. 6 (5), 581–586.

Muller, T., Bain, G., Wang, X., Papkoff, J., 2002. Regulation of epithelial cell migration and tumor formation by beta-catenin signaling.. Exp. Cell Res. 280 (1), 119–133.

Nakamura, T., Nishizawa, T., Hagiya, M., Seki, T., Shimonishi, M., Sugimura, A., Tashiro, K., Shimizu, S., 1989. Molecular cloning and expression of human hepatocyte growth factor. Nature 342 (6248), 440–443. doi:10.1038/342440a0.

Nishimura, K., Matsumiya, K., Miura, H., Tsujimura, A., Nonomura, N., Matsumoto, K., Nakamura, T., Okuyama, A., 2003. Effects of hepatocyte growth factor on urokinase-type plasminogen activator (upa) and upa receptor in du145 prostate cancer cells. Int. J. Androl. 26 (3), 175–179.

Organ, S.L., Tsao, M.-S., 2011. An overview of the c-met signaling pathway. Ther. Adv. Med. Oncol. 3 (1 Suppl), S7–S19. doi:10.1177/1758834011422556.

Petrelli, A., Gilestro, G.F., Lanzardo, S., Comoglio, P.M., Migone, N., Giordano, S., 2002. The endophilin-cin85-cbl complex mediates ligand-dependent downregulation of c-met. Nature 416 (6877), 187–190. doi:10.1038/416187a.

Pickup, M., Novit, S., Moses, H., 2013. The roles of tgf-beta in the tumour microenvironment. Nat. Rev. Cancer 13 (11), 788–799.

Potempa, S., Ridley, A.J., 1998. Activation of both map kinase and phosphatidylinositide 3-kinase by ras is required for hepatocyte growth factor/scatter factor-induced adherens junction disassembly. Mol. Biol. Cell 9 (8), 2185–2200.

Rejniak, K.A., McCawley, L.J., 2010. Current trends in mathematical modeling of tumor-microenvironment interactions: a survey of tools and applications. Exp. Biol. Med. (Maywood) 235 (4), 411–423. doi:10.1258/ebm.2009.009230.

Roletto, F., Galvani, A.P., Cristiani, C., Valsasina, B., Landonio, A., Bertolero, F., 1996. Basic fibroblast growth factor stimulates hepatocyte growth factor/scatter factor secretion by human mesenchymal cells. J. Cell Physiol. 166 (1), 105–111. doi:10.1002/(SICI)1097-4652(199601)166:1⟨105::AID-JCP12⟩3.0.CO;2-E.

Schatton, T., Frank, N.Y., Frank, M.H., 2009. Identification and targeting of cancer stem cells. Bioessays 31 (10), 1038–1049. doi:10.1002/bies.200900058.

Sick, S., Reinker, S., Timmer, J., Schlake, T., 2006. Wnt and dkk determine hair follicle spacing through a reaction-diffusion mechanism. Science 314 (5804), 1447–1450. doi:10.1126/science.1130088.

Sidenius, N., Blasi, F., 2003. The urokinase plasminogen activator system in cancer: recent advances and implication for prognosis and therapy. Cancer Metastasis Rev. 22 (2–3), 205–222.

Sottoriva, A., Verhoeff, J.J.C., Borovski, T., McWeeney, S.K., Naumov, L., Medema, J.P., Sloot, P.M.A., Vermeulen, L., 2010. Cancer stem cell tumor model reveals invasive morphology and increased phenotypical heterogeneity. Cancer Res. 70 (1), 46–56. doi:10.1158/0008-5472.CAN-09-3663.

Stella, M.C., Trusolino, L., Pennacchietti, S., Comoglio, P.M., 2005. Negative feedback regulation of met-dependent invasive growth by notch. Mol. Cell Biol. 25 (10), 3982–3996. doi:10.1128/MCB.25.10.3982-3996.2005.

Stoker, M., Perryman, M., 1985. An epithelial scatter factor released by embryo fibroblasts. J. Cell Sci. 77, 209–223.

Syed, Z.A., Yin, W., Hughes, K., Gill, J.N., Shi, R., Clifford, J.L., 2011. Hgf/c-met/stat3 signaling during skin tumor cell invasion: indications for a positive feedback loop. BMC Cancer 11, 180. doi:10.1186/1471-2407-11-180.

Talukdar, S., Kundu, S.C., 2012. A non-mulberry silk fibroin proten based 3d in vitro tumor model for evaluation of anticancer drug activity. Adv. Funct. Mater. 22 (22), 4778–4788.

Tanaka, K., Okigami, M., Toiyama, Y., Morimoto, Y., Matsushita, K., Kawamura, M., Hashimoto, K., Saigusa, S., Okugawa, Y., Inoue, Y., Uchida, K., Araki, T., Mohri, Y., Mizoguchi, A., Kusunoki, M., 2012. In vivo real-time imaging of chemotherapy response on the liver metastatic tumor microenvironment using multiphoton microscopy. Oncol. Rep. 28 (5), 1822–1830. doi:10.3892/or.2012.1983.

Trimboli, A.J., Cantemir-Stone, C.Z., Li, F., Wallace, J.A., Merchant, A., Creasap, N., Thompson, J.C., Caserta, E., Wang, H., Chong, J.-L., Naidu, S., Wei, G., Sharma, S.M., Stephens, J.A., Fernandez, S.A., Gurcan, M.N., Weinstein, M.B., Barsky, S.H., Yee, L., Rosol, T.J., Stromberg, P.C., Robinson, M.L., Pepin, F., Hallett, M., Park, M., Ostrowski, M.C., Leone, G., 2009. Pten in stromal fibroblasts suppresses mammary epithelial tumours. Nature 461 (7267), 1084–1091. doi:10.1038/nature08486.

Trusolino, L., Bertotti, A., Comoglio, P.M., 2010. Met signalling: principles and functions in development, organ regeneration and cancer. Nat. Rev. Mol. Cell Biol. 11 (12), 834–848. doi:10.1038/nrm3012.

Trusolino, L., Cavassa, S., Angelini, P., Andó, M., Bertotti, A., Comoglio, P.M., Boccaccio, C., 2000. Hgf/scatter factor selectively promotes cell invasion by increasing integrin avidity. FASEB J 14 (11), 1629–1640.

Turing, A.M., 1952. The chemical basis of morphogenesis. J. Philos. Trans. R. Soc. Lond. Ser. B Bio. Sci. B 237 (641), 37–72.

Ueoka, Y., Kato, K., Kuriaki, Y., Horiuchi, S., Terao, Y., Nishida, J., Ueno, H., Wake, N., 2000. Hepatocyte growth factor modulates motility and invasiveness of ovarian carcinomas via ras-mediated pathway. Br. J. Cancer 82 (4), 891–899. doi:10.1054/bjoc.1999.1016.

Ulisse, S., Baldini, E., Sorrenti, S., D'Armiento, M., 2009. The urokinase plasminogen activator system: a target for anti-cancer therapy. Curr. Cancer Drug Targets 9 (1), 32–71.

Verma, N., Keinan, O., Selitrennik, M., Karn, T., Filipits, M., Lev, S., 2015. Pyk2 sustains endosomal-derived receptor signalling and enhances epithelial-to-mesenchymal transition. Nat. Commun. 6, 6064. doi:10.1038/ncomms7064.

Vermeulen, L., De Sousa E Melo, F., van der Heijden, M., Cameron, K., de Jong, J.H., Borovski, T., Tuynman, J.B., Todaro, M., Merz, C., Rodermond, H., Sprick, M.R., Kemper, K., Richel, D.J., Stassi, G., Medema, J.P., 2010. Wnt activity defines colon cancer stem cells and is regulated by the microenvironment. Nat. Cell Biol. 12 (5), 468–476. doi:10.1038/ncb2048.

Wang, Z., Butner, J.D., Kerketta, R., Cristini, V., Deisboeck, T.S., 2015. Simulating cancer growth with multiscale agent-based modeling. Semin. Cancer Biol. 30, 70–78. doi:10.1016/j.semcancer.2014.04.001.

Watabe, T., Miyazono, K., 2009. Roles of tgf-beta family signaling in stem cell renewal and differentiation. Cell Res. 19 (1), 103–115. doi:10.1038/cr.2008.323.

Welter, M., Rieger, H., 2013. Interstitial fluid flow and drug delivery in vascularized tumors: a computational model. PLoS One 8 (8), e70395. doi:10.1371/journal.pone.0070395.

Wise, S., Lowengrub, J., Cristini, V., 2011. An adaptive multigrid algorithm for simulating solid tumor growth using mixture models. Math. Comput. Model 53 (1-2), 1–20.

Wise, S.M., Lowengrub, J.S., Frieboes, H.B., Cristini, V., 2008. Three-dimensional multispecies nonlinear tumor growth–i model and numerical method. J. Theor. Biol. 253 (3), 524–543. doi:10.1016/j.jtbi.2008.03.027.

Wong, A., Leung, P., Auersperg, N., 2000. Hepatocyte growth factor promotes in vitro scattering and morphogenesis of humanc cervical carcinomal cells. Gynocel. Oncol. 78 (2), 158–165.

Xiao, G.H., Jeffers, M., Bellacosa, A., Mitsuuchi, Y., Vande Woude, G.F., Testa, J.R., 2001. Anti-apoptotic signaling by hepatocyte growth factor/met via the phosphatidylinositol 3-kinase/akt and mitogen-activated protein kinase pathways. Proc. Natl. Acad. Sci. U S A 98 (1), 247–252. doi:10.1073/pnas.011532898.

Yamazaki, S., Skaptason, J., Romero, D., Lee, J.H., Zou, H.Y., Christensen, J.G., Koup, J.R., Smith, B.J., Koudriakova, T., 2008. Pharmacokinetic-pharmacodynamic modeling of biomarker response and tumor growth inhibition to an orally available cmet kinase inhibitor in human tumor xenograft mouse models. Drug Metab. Dispos. 36 (7), 1267–1274. doi:10.1124/dmd.107.019711.

Yan, H., Konstorum, A., Lowengrub, J., 2017. Three-dimensional spatiotemporal modeling of colon cancer organoids reveals that multimodal control of stem cell self-renewal is a critical determinant of size and shape in early stages of tumor growth. Bull. Math. Biol. (inpress).

Yan, H., Romero-Lopez, M., Frieboes, H.B., Hughes, C.C.W., Lowengrub, J.S., 2016. Multiscale modeling of glioblastoma suggests that the partial disruption of vessel/cancer stem cell crosstalk can promote tumor regression without increasing invasiveness. IEEE Trans. Biomed. Eng. doi:10.1109/TBME.2016.2615566.

Youssefpour, H., Li, X., Lander, A.D., Lowengrub, J.S., 2012. Multispecies model of cell lineages and feedback control in solid tumors. J. Theor. Biol. 304, 39–59. doi:10.1016/j.jtbi.2012.02.030.

Zeuner, A., Todaro, M., Stassi, G., De Maria, R., 2014. Colorectal cancer stem cells: from the crypt to the clinic. Cell Stem Cell 15 (6), 692–705. doi:10.1016/j.stem.2014.11.012.

Zhang, L., Lander, A.D., Nie, Q., 2012. A reaction-diffusion mechanism influences cell lineage progression as a basis for formation, regeneration, and stability of intestinal crypts. BMC Syst. Biol. 6, 93. doi:10.1186/1752-0509-6-93.